



## Benzohydroxamate and nitrobenzohydroxamate affect membrane order: Correlations between spectroscopic and molecular dynamics to approach tuberculosis

Lucas Thadeu Felipe Kokuszi <sup>a</sup>, Yago Mendes Paes <sup>b</sup>, Aline Loise Santana Faria <sup>a</sup>, Jesus Alvarado-Huayhuaz <sup>b</sup>, Maurício Dornelles Caldeira Balboni <sup>b</sup>, Marinalva Cardoso dos Santos <sup>a</sup>, Sandra Cruz dos Santos <sup>a</sup>, Juliano Rosa de Menezes Vicenti <sup>a</sup>, Alexandre Luis Parize <sup>c</sup>, Adriano Velasque Werhli <sup>b</sup>, Karina dos Santos Machado <sup>b,\*</sup>, Vânia Rodrigues de Lima <sup>a,\*</sup>

<sup>a</sup> Grupo de Investigação em Interações Moleculares em Membranas, Programa de Pós-Graduação em Química Tecnológica e Ambiental (PPGQTA), Escola de Química e Alimentos (EQA), 96203-900 Rio Grande, RS, Brazil

<sup>b</sup> COMBI-Lab, Grupo de Biologia Computacional, Centro de Ciências Computacionais, Universidade Federal do Rio Grande, Av. Itália, km 8, Campus Carreiros, 96203-900 Rio Grande, RS, Brazil

<sup>c</sup> Programa de Pós-Graduação em Química-PPGQ, Departamento de Química, Centro de Ciencias Físicas e Matemáticas-CFM, Universidade Federal de Santa Catarina-UFSC, Campus Universitário Trindade, Caixa Postal 476, Florianópolis, SC 88040-900, Brazil

### ARTICLE INFO

**Keywords:**  
Asolectin  
MLVs  
 $\text{PIM}_2$   
Tuberculosis  
Spectroscopy  
Molecular dynamics

### ABSTRACT

This work correlates the effects of benzohydroxamate (BH) and nitrobenzohydroxamate (NBH) anions in two membrane models which may be used for anti-tuberculosis (anti-TB) spectroscopic studies and/or computational studies. Firstly, the BH and NBH influence in the physico-chemical properties of soy asolectin (ASO)-based large multilamellar vesicles (MLVs) were evaluated by spectroscopic and calorimetric studies. In parallel, the BH and NBH interaction with a *Mycobacterium tuberculosis* (Mtb) inner membrane model, composed of phosphatidyl-myo-inositol-dimannoside ( $\text{PIM}_2$ ), was investigated by molecular dynamics (MD) simulations. Spectroscopic data showed a localization of BH close to the lipid phosphate group, while NBH was found close to the choline region. The BH ordered the ASO choline, phosphate and carbonyl regions and disrupted the acyl methylenes, reducing the membrane packing of the lipid hydrophobic region. On the other hand, NBH showed an ordering effect in all the lipid groups (polar, interface and hydrophobic ones). By MD studies, it was found that NBH enhanced the stability of the  $\text{PIM}_2$  membrane more than BH, while also being positioned closer to its mannose oxygens. As in ASO MLVs, BH was localized close to the  $\text{PIM}_2$  phosphate group and disrupted its acyl chains. However, higher values of lateral diffusion were observed for NBH than BH. Despite this, BH and NBH increased the membrane thickness by 35 %, which suggests a global ordering effect of both drugs. Findings of this work reinforce the accordance and complementarity between MLVs based on ASO and the  $\text{PIM}_2$  MD model results to study the drug effects in Mtb membrane properties.

### List of abbreviations

ASO	soy asolectin
BH	benzohydroxamate
CSA	chemical shift anisotropy
DLS	dynamic light scattering
DSC	differential scanning calorimetry

(continued on next column)

(continued)

FID	free induction decay
HATR-FTIR	horizontal attenuated total reflectance-Fourier transform infrared
<sup>1</sup> H NMR	hydrogen nuclear magnetic resonance
MD	molecular dynamics
Mtb	<i>Mycobacterium tuberculosis</i>
MDR-TB	<i>Mycobacterium tuberculosis</i> multidrug-resistance

(continued on next page)

\* Corresponding authors.

E-mail addresses: [karina.machado@furg.br](mailto:karina.machado@furg.br) (K. dos Santos Machado), [vania.lima@furg.br](mailto:vania.lima@furg.br) (V.R. de Lima).

(continued)

MLVs	large multilamellar vesicles
NBH	nitrobenzohydroxamate
NMR	nuclear magnetic resonance
PC	phosphatidylcholine
PDI	polydispersity index
$^{31}\text{P}$ NMR	phosphorus nuclear magnetic resonance
PIM <sub>2</sub>	phosphatidyl-myo-inositol-dimannoside
$R_H$	average hydrodynamic radius
T <sub>m</sub>	phase transition temperature
T <sub>1</sub>	spin-lattice relaxation time
RMSD	root mean square deviation
TB	tuberculosis
TSP	3-(trimethylsilyl)-[2,2,3,3-2H4]-1-propionate
$\Delta H$	enthalpy variation
$\nu_{\text{as}} \text{N}^+(\text{CH}_3)_3$	antisymmetric stretching of choline
$\nu_{\text{as}} \text{PO}_2$	phosphate
$\nu_{\text{COC}}$	stretching vibrations of ester
$\nu_{\text{C=O}}$	stretching vibrations of carbonyl
$\nu_s \text{CH}_2$	symmetric stretching vibrations of methylene
$\nu_{\text{as}} \text{CH}_2$	antisymmetric stretching vibrations of methylene
$\zeta$	zeta potential

## 1. Introduction

*Mycobacterium tuberculosis* (Mtb) multidrug-resistance (MDR-TB), attributed to the obsolete and prolonged period of TB therapy, is considered a health security threat and has an important role in the worldwide public health crisis [1–4]. In 2020, only a third of people infected with MDR-TB had access to drug therapy to fight the disease [5]. MDR-TB is related to the cell wall of the Mtb complex, which is rich in lipids, such as phosphatidyl-myo-inositol-dimannosides (PIM<sub>2</sub>) and mycolic acid [4,6,7], and it provides an impermeable hydrophobic barrier against drug entrance [8,9]. Thus, it is important to note and consider the advances for new anti-TB drug development and drug repurposing [10], including that related to cell wall perturbation in Mtb.

In the context of new anti-TB drug development, benzohydroxamic acids and their corresponding anions (such as benzohydroxamate anion, BH, and *m*-nitrobenzohydroxamate anion, NBH—both shown in Fig. 1) have been reported as promising substances to achieve this development [11]. These compounds have demonstrated the ability to bind to metal ions, to inhibit the activities of ureases and metalloproteinases, and also to compete against bacterial siderophores for Fe<sup>3+</sup> [12,13]. Complexes containing NBH ligands associated with copper and cobalt affected the growth of *M. tuberculosis*, showing an intracellular activity comparable to rifampicin [14]. In light of these findings, the quantum mechanics calculation is an important and widely used tool to estimate the global reactivity and to identify intermolecular interactions of small molecules, such as BH and NBH [15,16].

The phosphatidylcholine-based liposomes have been used to improve hydroxamic acid solubility, *in vitro* release and *in vivo* pharmacokinetics [17,18]. Beyond their role in the development of drug delivery systems, the liposomes may be useful to furnish important data concerning the drug's mechanisms of actions [3]. In the case of TB, a deeper comprehension of the interaction dynamics between Mtb cell

envelope components and potential drugs or active substances is important for developing new effective therapeutic strategies [19]. Phospholipid-based liposomes have been used as a simplified-model to understand the role of anti-TB drugs in Mtb cell envelope permeability [20]. A spectroscopic characterization of liposomes provides information related to the degree of hydration of the system, freedom of vibrational and rotational movements, *trans-gauche* isomerization and chemical shift anisotropy [21,22]. Besides spectroscopic characterization, molecular dynamics (MD) simulation is one of the most widely used approaches to understand both the behavior of cell membrane and drug interactions [23]. In previous work [3], our research group used the physico-chemical characterization of large multilamellar vesicles (MLVs) composed by soybean asolectin (ASO, which contains mainly phosphatidylcholine, phosphatidylethanolamine and phosphatidylinositol phosphate) and mefloquine to validate an Mtb inner membrane model composed of phosphatidyl-myo-inositol-dimannoside (PIM<sub>2</sub>) built for MD simulations. The composition of ASO phospholipids shows structural similarities with the PIM<sub>2</sub> membrane in the polar, interfacial and hydrophobic regions. Our results showed very similar locations and effects in both membrane models, promoting a reliable comparison between them, which was correlated to the efficiency of mefloquine synergism with anti-TB drugs against Mtb drug-resistant strains. The application of MD becomes a fundamental tool for the study of TB (from membrane models) in order to elucidate complementary information about the mechanism of action and synergism of drugs against Mtb [3].

This work aims at assessing the effects of benzohydroxamate (BH) and nitrobenzohydroxamate (NBH) anions in ASO MLVs and PIM<sub>2</sub> membrane models, with a focus on their influence on membranes physico-chemical properties (such as size, thickness, hydration degree, lipid motions, order, isomerization, transition states, enthalpy variation, lateral diffusion, and atomic distances, among others), location and also structural stability for potential applications in anti-tuberculosis (anti-TB) drug development.

Thus, the effects of BH and NBH in the membranes were investigated by spectroscopic and MD characterizations. Spectroscopic data was obtained from ASO MLVs systems containing BH and NBH anions, through horizontal attenuated total reflectance-Fourier transform infrared (HATR-FTIR), nuclear magnetic resonance (NMR), dynamic light scattering (DLS), differential scanning calorimetry (DSC) and zeta potential ( $\zeta$ ) techniques. The MD studies were used to report the interaction of these anions with the PIM<sub>2</sub> membrane model by analyses of the root mean square deviation (RMSD), partial mass density, atomic distances, deuterium order parameters, lateral diffusion and membrane thickness [3]. Results were discussed in order to find correlations between the ASO MLVs and the PIM<sub>2</sub> MD models that may be useful for studying the BH and NBH effects in the physico-chemical properties of Mtb membrane and develop new anti-TB drug delivery systems.

## 2. Materials and methods

### 2.1. Materials

ASO (containing L-a-phosphatidylcholine), tricine, magnesium

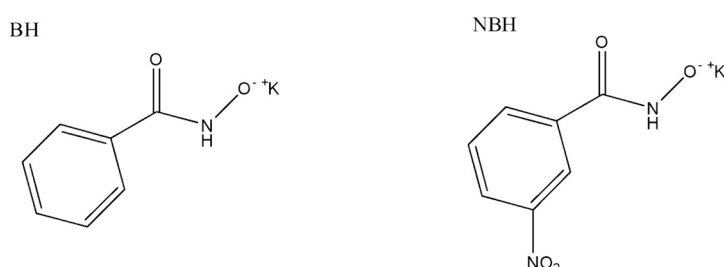


Fig. 1. Structures of benzohydroxamate (BH) and *m*-nitrobenzohydroxamate (NBH) anions.

chloride, and deuterated water containing sodium 3-(trimethylsilyl)-[2,2,3,3-2H4]-1-propionate (TSP, 0.05 %) were purchased from Sigma-Aldrich (St. Louis, MO, USA). Lipids were used without further purification, whereas all other chemicals were of analytical grade.

## 2.2. Synthesis of BH and NBH

The potassium salts of BH and NBH were synthesized and kindly donated by Juliano Vicenti, Ph.D. The synthesis procedures to obtain the BH and NBH used in this work are described and characterized in the work of Lisboa and colleagues [12]. Briefly, a methanolic hydroxylamine solution containing potassium hydroxide was prepared. In this reaction medium, a solution of ethyl benzoate (for the synthesis of BH) or ethyl 3-nitrobenzoate (for the synthesis of NBH), previously prepared in methanol, was added. The mixture was stirred at room temperature and evaporated under vacuum. Then, the solid of BH or NBH was washed with chloroform.

## 2.3. MLV preparation

The preparation of MLVs was performed using the reverse-phase evaporation method [24,25]. To obtain the control samples, ASO 50 mg·mL<sup>-1</sup> was briefly dissolved in chloroform and dispersed in a tricine 10 mM/MgCl<sub>2</sub> 2.5 mM aqueous buffer, pH 7.4. The mixture was sonicated in a bath sonicator, followed by chloroform evaporation under reduced pressure. The resulting organogel was resuspended and hydrated in 1 mL of the tricine/MgCl<sub>2</sub> buffer. To obtain the ASO MLVs dispersion containing BH and those containing NBH (both at 5 mg·mL<sup>-1</sup>, corresponding to 10 % of the lipid concentration, or a drug:lipid ratio of 1:10, m/m), the drugs were previously solubilized in a tricine/MgCl<sub>2</sub> buffer and added in the organogel hydration step. Thus, the proportion of BH and NBH molecules in the buffer solution was approximately 1:10.

## 2.4. DLS measurements and zeta potential ( $\zeta$ )

The average hydrodynamic radius ( $R_H$ ) and electrophoretic mobility measurements of the ASO MLVs dispersions, i.e. controls and the samples containing BH and NBH, were determined using a Zetasizer Malvern UK-Nano ZS instrument (Malvern Instruments Ltd., Worcestershire, England). To determine size distribution by DLS, samples were diluted 40 times with ultrapure water and analyzed in an optical grade polystyrene cuvette at 25 °C. Intensity correlation functions were measured at a scattering angle of  $\theta = 173^\circ$ , using a wavelength of 488 nm. All reported hydrodynamic radii were calculated using the Stokes-Einstein equation. Samples for zeta potential assays were prepared by diluting 25 µL of the MLVs controls and samples containing BH or NBH in 1 mL Milli-Q water and submitted to vortex for 1 min. The zeta potential was measured ten times in each experiment and the mean zeta potential values were calculated from three replicates [26].

## 2.5. Spectroscopic characterization of the MLVs systems

### 2.5.1. HATR-FTIR measurements

HATR-FTIR spectra of the MLVs-loaded BH and NBH samples, and their respective controls (without the drugs), were obtained using a Shimadzu-IR Prestige-21 spectrophotometer (Kyoto, Japan). Interferograms were obtained by an average of 45 scans (resolution equivalent to 2 cm<sup>-1</sup>) and registered from 4000 to 400 cm<sup>-1</sup> [27]. The obtained spectra were analyzed according to the BH and NBH-induced shifts on the wavenumber of peaks related to the axial stretching vibrations of the ASO groups [21]. The observed peaks were attributed to the antisymmetric stretching of choline ( $\nu_{as}$  N<sup>+</sup>(CH<sub>3</sub>)<sub>3</sub>) and phosphate groups ( $\nu_{as}$  PO<sub>2</sub><sup>-</sup>), the stretching vibrations of ester ( $\nu$  COC) and carbonyl ( $\nu$  C=O) groups and also the symmetric and antisymmetric stretching vibrations of methylene,  $\nu_s$  CH<sub>2</sub> and  $\nu_{as}$  CH<sub>2</sub>, respectively.

### 2.5.2. NMR measurements

<sup>1</sup>H NMR spin-lattice relaxation times (T<sub>1</sub>), as well as <sup>31</sup>P NMR spectra chemical shift anisotropy (CSA), were measured using Bruker Avance DRX 400 NMR (Ettlingen, Germany) equipment at 400 and 161 MHz, respectively, at 25 °C. For both assays, controls and samples were dispersed in a water:deuterated water (80:20, v/v) solution. The <sup>1</sup>H T<sub>1</sub> values related to lipid choline (3.2 ppm) and methylene (1–2 ppm) groups were obtained using the inversion recovery sequence at recovery times ranging between 0.4 and 12.8 s, followed by exponential data fitting to the NUTS code. <sup>31</sup>P NMR spectra were measured using a recycling time of 4 s, a delay of 0.2 s, and an acquisition time of 0.5111808 s. For each sample, 2048 scans were accumulated. The overall CSA was obtained from the difference between parallel and perpendicular chemical tensors, measured on the <sup>31</sup>P NMR spectrum [22,28].

### 2.5.3. DSC measurements

DSC assays of the samples were performed by Shimadzu DSC-60 equipment (Tokyo, JP). The heating rate was set to 10 °C/min in a temperature range from –45 to 5 °C, under nitrogen flow (50/50 mL/min) [29–31]. An empty aluminum pan was used as a reference [32, 33]. The enthalpy variation ( $\Delta H$ ) was obtained by integrating the area under the DSC peak with TA 60WS software [34,35].

### 2.5.4. Statistical analyses

In all spectroscopic experiments, results were shown as the mean of triplicates from three independent experiments.

## 2.6. Molecular dynamics

The potential effects of BH and NBH on the membrane of *M. tuberculosis* were analyzed by conducting molecular dynamics simulations (MD) using the GROMACS 2022 package [36]. GROMACS is a popular software package utilized to simulate biochemical molecules such as proteins, lipids and nucleic acids. The membrane model used in this work was proposed by Scaini and colleagues [37]. For generating 3D configurations and minimized conformations of the hydroxamate molecules, Avogadro software was used [38]. The lipid molecule, along with both BH and NBH, was subsequently processed using CHARMM-GUI [39] to apply the CHARMM36 [40,41] force field and get molecular parameters for running the simulations.

Three MD simulations were performed: membrane in water (PIM<sub>2</sub> control), membrane in water with BH (PIM<sub>2</sub>-BH) and membrane in water with NBH (PIM<sub>2</sub>-NBH). Each system consisted of two lipid layers containing 64 molecules of PIM<sub>2</sub> arranged perpendicularly to the Z-axis. Additionally, there was one waterbox on each side of the constructed membrane with 6 molecules of each of the corresponding molecules BH and NBH. This proportion of BH and NBH molecules to lipids in the PIM<sub>2</sub>-BH and PIM<sub>2</sub>-NBH systems was set to approximately 10 % (1,10) to align the simulations with the experimental conditions.

For all the systems, it was performed energy minimizations with the steepest-descent algorithm, equilibrations (NVT and NPT for 10 ns) with restraints for the lipid phosphorus in the Z-axis and the production of MD simulation with restraints only for h-bonds for 100 ns, with the temperature adjusted to 310 K. Further information was described in Section 1.1 of the supplementary material of this article.

## 3. Results and discussion

In this paper, results were organized and shown in order to describe the influence of BH and NBH in specific regions of two different membrane models. Furthermore, each technique used in this paper provided information related to a membrane physico-chemical parameter that complements or reinforces the remaining parameters measured, in order to obtain a global effect of the BH and NBH in ASO MLVs and in the PIM<sub>2</sub> model.

### 3.1. BH and NBH influence lipid self-assembly: studies with ASO MLVs

#### 3.1.1. BH and NBH effects on MLV size

The results of the average hydrodynamic radius ( $R_H$ ) and polydispersity index (PDI) of the ASO MLVs, in the absence and presence of BH and NBH, are available in Table 1.

The PDI values obtained for ASO, ASO + BH and ASO + NBH varied from 0.67 to 0.78, indicating heterogeneity in the MLV systems. This heterogeneity obtained is associated with the method of preparation of the MLVs, generating populations of different sizes [42]. Furthermore, it is probable that the obtained range of PDI makes the analysis by DLS less reliable. Thus, the size results obtained by DLS may be inconclusive. However, considering the difference between the  $R_H$  obtained for ASO and NBH, some hypotheses may be contemplated. The  $R_H$  obtained for ASO was  $152.35 \pm 5.23$  nm, and after the insertion of BH and NBH into the system, an increase of 23.5 % and 64.1 %, respectively, was observed. The greater variation observed in NBH (along the lower value of PDI) may also be due to an interaction between the nitrobenzene groups and those located in the ASO polar region. This may alter the flexibility of the ASO polar head arrangement of the outer monolayer of the vesicle, since the lipid shows a hexagonal phase, affecting the dipole-dipole interactions aligning neighboring moieties [25,43,44]. It is also known that the interaction, location and orientation of a molecule inside a MLV influence its core, curvature and size [45,46]. Thus, despite the fact that these size variations may be a reflection of the system heterogeneity, it is also possible that BH and NBH have distinct locations and orientations in the ASO MLVs. Previous studies of our research group [45] demonstrated that the transverse distribution of quercetin was responsible for a 70.5 % increase in the size of ASO liposomes. It is important to know that the aromatic ring current effect in the delocalized  $\pi$ -electrons of benzenes is a tool to reflect an axial or transverse molecular orientation of a molecule, with respect to the lipid [47]. NMR studies indicated that aromatic polar substituents have a strong influence on the ring current effect, and this may determine the molecular orientation toward the membrane surface in aqueous media [48–50]. Thus, considering that BH and NBH differ structurally by a nitro group, these results generated the question: how is the presence of the nitro group responsible for a differential orientation in the NBH molecule compared to the BH?

#### 3.1.2. BH and NBH influence on specific regions of MLVs—spectroscopic data

The influence of BH and NBH on specific regions of lipid membranes is reported in the following. It is important to note that the behavior reported in each region of the membrane after the interaction with BH and NBH was investigated considering specific physico-chemical parameters, such as hydration degree, translational and collisional motions, rotation rate, trans-gauche isomerization, transition states and enthalpy variation, as described below.

**3.1.2.1. Effects in the polar region of membranes.** The BH and NBH influences on the vibrational and rotational properties of specific regions of MLVs were investigated by HATR-FTIR and are shown in Fig. 2. From

**Table 1**

Average hydrodynamic radius ( $R_H$ ) and polydispersity index (PDI) for pure asolectin large multilamellar vesicles (ASO MLVs) and MLVs containing BH and NBH (ASO + BH and ASO + NBH). The values are shown as mean  $\pm$  standard deviation ( $n = 3$ ).

MLV systems	$R_H$ (nm)	PDI
ASO	$152.35 \pm 5.23$	$0.76 \pm 0.10$
ASO + BH	$188.15 \pm 6.35$	$0.78 \pm 0.05$
ASO + NBH	$250.01 \pm 15.45$	$0.67 \pm 0.16$

Potassium benzohydroxamate (BH) and potassium m-nitrobenzohydroxamate (NBH).

the spectra shown in Fig. 2, the peak wavenumber and bandwidth variations induced by BH and NBH in the specific regions of ASO were calculated and are described in Fig. 3.

Considering the  $2\text{ cm}^{-1}$  resolution of the equipment, FTIR information related to BH and NBH effects on polar lipid regions were monitored, discussed and complemented by NMR and zeta potential data as shown hereafter.

**3.1.2.1.1. Effects on lipid choline.** No effects in the  $\nu_{as} N^+(CH_3)_3$  peak wavenumber induced by BH were observed (Fig. 3A). On the other hand, an increase of  $19.29\text{ cm}^{-1}$  the  $\nu_{as} N^+(CH_3)_3$  peak wavenumber indicates that NBH disrupts the dipole-dipole interactions between choline and the phosphate group located in the neighboring lipid molecule [21,32,34]. This is related to the ion-dipole, dipole-dipole and  $\pi$ -cation interactions between the carbonyl, nitro and/or benzene groups of NBH and the quaternary ammonium of the choline [21,50–54]. The  $\nu_{as} N^+(CH_3)_3$  bandwidth was not affected by BH nor by NBH.

In order to investigate the impact of BH and NBH on the choline rotation rate and their potential influence in the behavior observed by FTIR, NMR  $T_1$  data were calculated from the recovery of the choline  $^1\text{H}$  free induction decay (FID) signals (please see the supplementary material of this article, Fig. S2 and Table S1). The insertion of BH into the ASO MLVs promoted a 16 % decrease in  $T_1$  values, from 0.68 s to 0.57 s, indicating a higher rotation rate (and higher mobility, consequently) of the choline group [52,55]. It is due to the fact that a decrease in  $T_1$  values induces a decrease in correlation time ( $\tau_c$ ), which has an inverse relationship with mobility [3,56]. In contrast, NBH increased ASO choline  $T_1$  values by 31 %, from 0.68 s to 0.89 s, reflecting lower molecular mobility of the choline group [34,57]. The ordering effect promoted by NBH in ASO choline is probably due to dipolar interactions between the nitro and amine groups of NBH with choline and/or the benzene ring and choline by  $\pi$ -cation interactions. These interactions may interfere with the electrostatic attraction forces between the phosphate group of the ASO and the neighboring lipid choline group [3], reflecting in the wavenumber shift observed in the FTIR  $\nu_{as} N^+(CH_3)_3$  peak.

**3.1.2.1.2. Effects on lipid phosphate.** BH and NBH did not promote variations in the wavenumber of  $\nu_{as} PO_2^-$ , which indicates no changes in the degree of hydration of the lipid phosphate (Fig. 3A) [21,58]. The insertion of BH and NBH into the MLV promoted a decrease in  $\nu_{as} PO_2^-$  bandwidth values, by  $1.16$  and  $0.72\text{ cm}^{-1}$ , respectively (Fig. 3B). It is important to note that changes in the FTIR bandwidth of the lipid are influenced by translational, rotational and/or collisional effects in the presence of an exogenous substance, and they have a direct relationship to the speed of molecular movement [21,34,59,60]. The results have shown that both BH and NBH were responsible for a restriction of the mobility of the lipid phosphate group, with the stronger effect being observed in the BH. These restrictions may be related to the fact that the hydroxylamine amine group ( $NHCOO^-$ ) present in both BH and NBH could be performing hydrogen bonding and/or ion-dipole interactions with the lipid phosphate group [61,62]. By promoting an additional repulsive force compared to BH, the electronegative character of the nitro group ( $NO_2$ ) [50] may be responsible for the NBH-induced shift in the lipid  $\nu_{as} PO_2^-$  bandwidth being 1.61 times (or about 62 %) smaller than the BH. This may define the orientation of the NBH molecule to the MLV surface, corroborating with the FTIR analyses of  $\nu_{as} N^+(CH_3)_3$ . As performed in choline studies, the effects of the BH and NBH on the phosphate rotation rate were monitored by NMR. The  $^{31}\text{P}$  NMR spectra are shown in Fig. 4.

From Fig. 4, information related to the phase state, nuclear Overhauser effect (NOE) and the chemical shift anisotropy (CSA) of the chemical environment of the  $^{31}\text{P}$  core [63–65] was obtained. All the  $^{31}\text{P}$  NMR spectra show a high-field shoulder ( $\perp$ ) and an intense low-field peak ( $\parallel$ ), as well as an isotropic peak, all of which are typical in an inverted hexagonal phase ( $H_{II}$ ) lipid arrangement [66,67]. The  $H_{II}$  phase is attributed to the arrangement of the ASO phosphatidylethanolamine content [45,65]. From the spectra analyses, one can observe that the

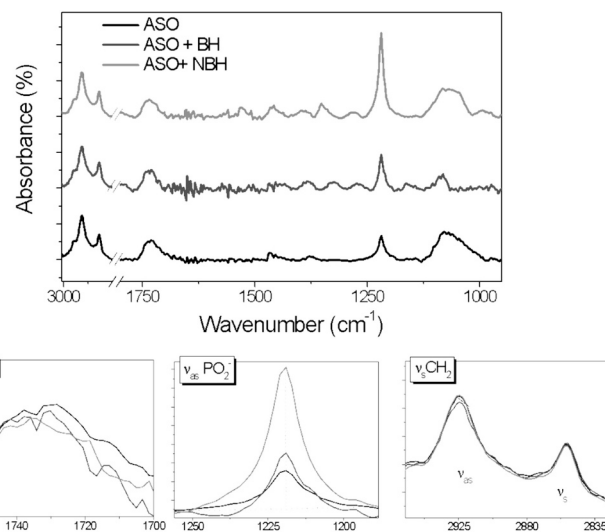


**Fig. 2.** Full HATR-FTIR spectra of empty asolectin large multilamellar vesicles (control, ASO MLVs) and ASO MLVs containing benzohydroxamate (ASO + BH) and m-nitrobenzohydroxamate (ASO + NBH). Below the full spectra, one can observe the zooms of HATR-FTIR spectra in the antisymmetric phosphate the stretching ( $\nu_{\text{as}} \text{PO}_2^-$ ), carbonyl stretching mode ( $\nu \text{C=O}$ ) and symmetric and antisymmetric stretching of acyl chain methylene ( $\nu_s \text{CH}_2$ ) regions.

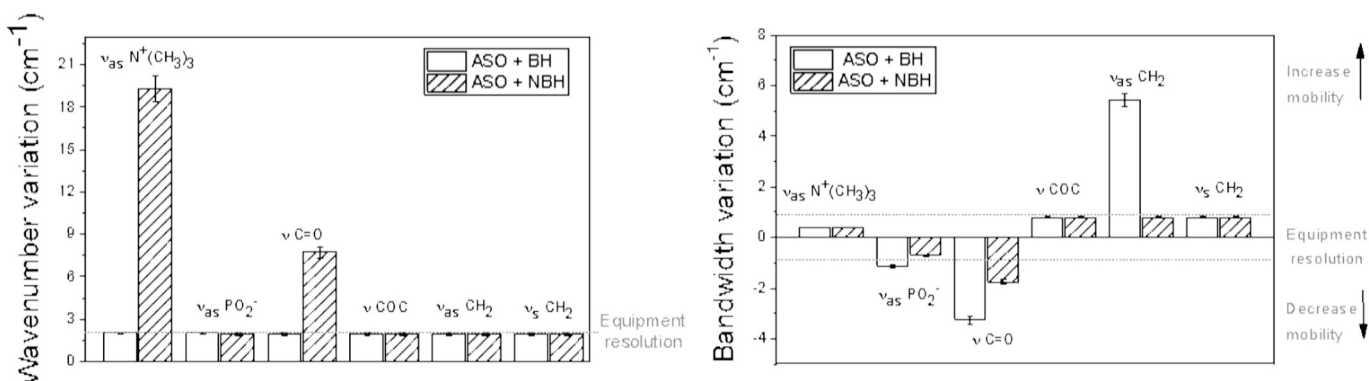


**Fig. 3.** FTIR wavenumber (A) and bandwidth (B) variations promoted by benzohydroxamate (ASO + BH) and m-nitrobenzohydroxamate NBH (ASO + NBH) in the stretching vibrations of specific groups of asolectin large multilamellar vesicles (ASO MLVs).

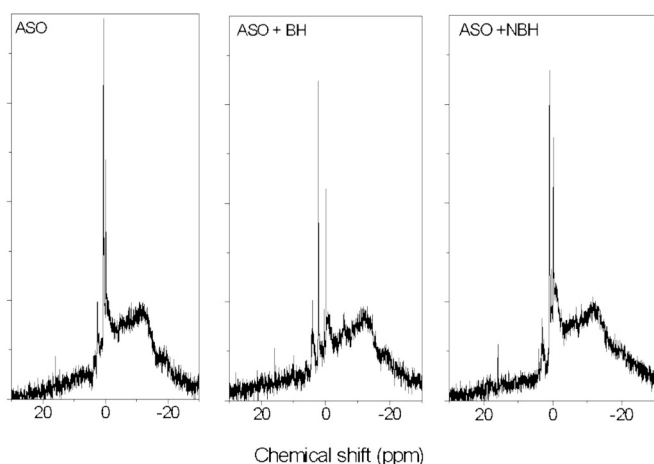


**Fig. 4.**  $^{31}\text{P}$  NMR spectra of asolectin large multilamellar vesicle controls (ASO MLVs) and those containing benzohydroxamate (ASO + BH) and m-nitrobenzohydroxamate NBH (ASO + NBH).  $^{31}\text{P}$  NMR measurements were recorded at 161 MHz, using water:deuterated water (80:20, v/v) as a reference. DS = 4 and NS = 2048.

insertion of BH and NBH does not change the ASO lipid phase state. The  $^{31}\text{P}$  spectra low-field peak (||) intensity is related to a NOE, which reflects the dipolar interaction between the lipid phosphate group and hydrogens from the aqueous medium [64,68].

Both BH and NBH induced a decrease in the intensity of the low-field peak (||), which reflects that the drugs reduce the interaction between phosphate and water. Consequently, this reduction reinforced the electrostatic interactions between the phosphate and neighboring choline groups [28]. It seems that BH had more influence on the  $^{31}\text{P}$  NOE than NBH. Thus, the BH seems to have a stronger interaction with the lipid phosphate group than NBH, reducing its interaction with water hydrogens. On the other hand, the stronger effect of NBH in the lipid choline region, observed by FTIR and  $^1\text{H}$  NMR, indicates that BH and NBH have distinct locations in the ASO polar region and reinforces the fact that the presence of the nitro group in the NBH reorients the molecule to the MLV surface.

The influence of the BH and NBH in the CSA of the  $^{31}\text{P}$  lipid core was investigated with the calculation of the spectra line widths (please see Table S1 of the supplementary material). The insertion of BH and NBH into the ASO MLVs increased the width of the  $^{31}\text{P}$  NMR peak by 3.84 and 0.2 ppm, respectively. Since phosphorus CSA variations reflect changes in the rotational motion and, consequently, in the  $^{31}\text{P}$  NMR peak width in an inversed relationship [28,56], the BH reduced the phosphorus rotation rate, promoting an ordering effect of the lipid phosphate group.

This effect reflects electrostatic interactions between the BH amine and the lipid phosphate group [61,69,70]. The influence of NBH on  $^{31}\text{P}$  NMR linewidth was 19.2 times smaller than that promoted by BH. These results corroborate with the FTIR bandwidth data of  $\nu_{\text{as}} \text{PO}_2^-$ . Since NBH carries an amine group, such as BH, which also may interact with the lipid phosphate, it is possible that this result is a consequence of the BH and NBH effects in membrane orientation. To evaluate the effect of BH and NBH in the molecular orientation and surface charge of the ASO polar region,  $\zeta$ -potential analyses were performed.

With respect to the ASO system, the  $\zeta$ -potential obtained was  $-64.50 \pm 2.92$  mV, typical of a phospholipid-based system [71], and after the insertion of BH and NBH into the system, the  $\zeta$ -potential values became more negative:  $-74.00 \pm 0.52$  mV (a variation of approximately 9.5 mV) and  $-72.80 \pm 3.25$  mV (a variation of approximately 8.3 mV), respectively. In the case of phosphatidylcholine, which represents 25 % of the ASO phospholipid composition, a negative  $\zeta$ -potential can be observed when the plane of the phosphate group lies above the plane of the choline group, and vice versa. Here, it is important to note that the headgroup of phosphatidylcholines is aligned to the surface in a way in that the vector connecting the phosphorus of the phosphate group and the nitrogen of the choline group is more than 30° lower than the bilayer plane [26,72]. The obtained variation in  $\zeta$ -potential values is related to the fact that both BH and NBH reorient the phosphate group to a position above the plane of the choline group in the MLV system [26,45]. The variation observed in NBH indicates a smaller effect on lipid phosphate reorientation that is promoted by BH. This reinforces a stronger effect in the choline group caused by NBH.

**3.1.2.2. Effects in the membrane interface.** Regarding the lipid interface region, analyses of BH/NBH-induced FTIR peak variations (Fig. 3) revealed that BH caused no changes in the ASO  $\nu \text{C=O}$  wavenumber but promoted a decrease of  $3.27 \text{ cm}^{-1}$  in its bandwidth. The NBH increased the wavenumber of  $\nu \text{C=O}$  by  $7.71 \text{ cm}^{-1}$  and decreased its bandwidth by  $1.76 \text{ cm}^{-1}$ . It is known that the  $\nu \text{C=O}$  wavenumber is sensitive to changes in the number of hydrogen bonding or in the polarity of the lipid carbonyl group [73]. On the other hand, the motion rate and conformational changes in the interfacial region of the membrane are reflected in proportional variations in the  $\nu \text{C=O}$  bandwidth [34,60,74]. Thus, the results showed that only NBH induced a change in the degree of lipid carbonyl hydration, reducing the number of hydrogen bonds on it [45,50,75]. This may due to an interaction between the lipid carbonyl group and the amine groups of the NBH hydroxylamine portion. Since both BH and NBH contain the hydroxylamine group, the apparent absence of this interaction related to BH reinforces that BH and NBH have different locations and orientations in the membrane. Bandwidth results indicated that, despite both BH and NBH decreasing the mobility of the lipid carbonyl group, BH showed an effect 1.86 times stronger than NBH in this restriction. It is known that aromatic rings usually show a preferential location in the interface region of lipid membranes [45,76]. Therefore, besides the different locations of both hydroxamates in the membrane, it is possible that the attractive forces related to the benzene group of both BH and NBH within the lipid groups also have different intensities. If that is the case, a pi-cation interaction between the NBH ring and the lipid choline group may have affected the carbonyl interactions and package in the membrane, enhancing its mobility when compared to the membrane after BH insertion.

**3.1.2.3. Effects in the membranes hydrophobic region.** The data concerning the HATR-FTIR bands of the methylene chain (Figs. 2 and 3) revealed no significant variations induced by BH or NBH in the wavenumber of ASO  $\nu_s \text{CH}_2$  and  $\nu_{\text{as}} \text{CH}_2$  peaks. This indicates that BH and NBH did not provoke changes in the motion rate of the acyl chain methylenes by *trans-gauche* isomerization [55,77–79]. Additionally, BH promoted an increase of  $5.42 \text{ cm}^{-1}$  in the FTIR bandwidth of ASO  $\nu_{\text{as}} \text{CH}_2$ , whereas NBH did not cause bandwidth variations in the peaks

related to  $\nu \text{CH}_2$ . It is known that, for the  $\nu \text{CH}_2$  peaks, an induced bandwidth variation promoted by an exogenous substance reflects changes in the motion freedom of methylenes, *trans-gauche* isomerization, frequency distribution along the chain and librotorsional mobility [34,78,80]. Thus, considering that BH did not affect the FTIR  $\nu \text{CH}_2$  wavenumber, the increase in the  $\nu_{\text{as}} \text{CH}_2$  bandwidth is attributed to a higher rate of liberation and twisting motions induced by BH.

NMR data related to the  $^1\text{H}$  T<sub>1</sub> of lipid methylenes (please see Fig. S2 and Table S1 in the supplementary material of this article) showed that BH promoted a 21 % decrease in T<sub>1</sub> values (from 0.67 s to 0.53 s). On the other hand, the insertion of NBH into the ASO MLVs promoted a 22 % increase in T<sub>1</sub> values (from 0.67 s to 0.82 s). The BH-induced decrease in the  $^1\text{H}$  T<sub>1</sub> of lipid methylenes indicates an increase in the rotational motion on the axis diffusion tensor related to the apolar region of the lipid, as well as the reorientation of the axis [3,81,82]. Thus, considering the FTIR results, it is possible to associate the increase of the mobility of the ASO acyl chain with the BH-induced increase in the rate of lipid rotational, librational and twisting motions. Considering the fact that the *trans-gauche* isomerization does not play a definitive role in the increase of lipid mobility (according to the FTIR data), the benzene ring of BH may act as a “spacer” between the acyl chain methylenes, decreasing their packing and order of the lipid self-assembly [45,49,83]. The opposite effect in lipid mobility, restriction, observed in NBH results, may be related to the reorientation of the nitro group caused by its interaction with the lipid choline, which also reallocates the NBH benzene group, thereby reducing its “spacer” effect in the lipid acyl chains. Furthermore, the Van der Waals interactions between the NBH nitro group and the lipid choline reinforce the alignment of the lipid portions neighboring the phosphate and choline groups, which may increase the packing of the lipid acyl chains [84].

The influence of BH and NBH in the phase transition temperature (T<sub>m</sub>) and ΔH was detected by the analysis of DSC curves (shown in Fig. S3, in the supplementary material of this article). BH did not promote a significant variation in the ASO T<sub>m</sub> (which varied from  $-23.06$  to  $-23.12$  °C) but reduced approximately 50 % of the lipid ΔH value (from  $-0.07$  to  $-0.03$  J/g). On the other hand, the NBH promoted a discreet but significant increase of the ASO T<sub>m</sub> value, equivalent to  $|0.21|$  °C (from  $-23.06$  to  $-22.85$  °C), and promoted a ΔH variation similar to that observed in BH (from  $-0.07$  to  $-0.02$  J/g).

The DSC results showed that the effect of BH and NBH in the lipid acyl chains is indirect and a consequence of their interactions with the polar interfacial regions of lipids. BH did not influence the ASO T<sub>m</sub> value, which is related to the *trans-gauche* isomerization of methylenes [79]. Thus, DSC data also corroborate the absence of variations observed in the ASO  $\nu \text{CH}_2$  wavenumber (please see the FTIR data in this section) after the insertion of BH. The increase of  $|0.21|$  °C in the ASO T<sub>m</sub> with NBH indicates a discreet ordering effect in the first acyl chain methylenes, probably as a consequence of NBH pi-cation interaction with the lipid choline group, discussed above [50,51,54]. Since *trans-gauche* isomerization reflects changes in T<sub>m</sub> values, the DSC results for NBH are in agreement with the  $^1\text{H}$  NMR data, suggesting that NBH affects and restricts the rate of the rotational motion of acyl chains. Considering the postulations of Jiao and colleagues [85], an interpretation of the ΔH variations promoted by BH and NBH reinforces the presence of electrostatic interactions between these substances and the ASO polar region. These interactions are related to BH with the lipid phosphate group, and NBH with the choline group, as shown in the FTIR and NMR results.

Based on the presented results in Table 1 and Figs. 2–4, it was compared the effects of BH and NBH in the ASO membrane. Spectroscopic data showed that BH and NBH increase the MLV size, and the effect of NBH was about 41 % more expressive than BH (please see Table 1). The lipid choline group is affected almost two times more by NBH than BH; the former restricted choline mobility and the latter increased its rotational motion. Both BH and NBH restricted the motion of the ASO phosphate group, and BH affected the mobility of this group

62 % more than NBH, also showing stronger dipolar interactions with this lipid region (Figs. 2 and 3). Specifically, BH decreased the rotational motion of the lipid phosphate group 19 times more than NBH (please see Fig. 4). Along the  $\zeta$ -potential values, results showed a preferential location of BH close to the phosphate group and, for NBH, near the choline group. Both BH and NBH restricted the motion of lipid interface, with BH showing a stronger effect in this region, affecting it two times more than NBH. In turn, NBH reduced the degree of lipid carbonyl hydration, and this parameter was not affected by BH. BH increased the motional freedom of the ASO hydrophobic region, but it seems that the influence of *trans-gauche* isomerization in this process is very small. NBH restricted the mobility of the lipid acyl chains. The results also indicated that BH is preferentially located close to the phosphate group and NBH is near the choline region, and their effects in interface and hydrophobic regions of the membrane are consequences of their interactions with the lipid polar groups. In order to compare the effects of BH and NBH in two membrane models which can be used for the design and development of anti-TB drugs and systems, the effects of BH and NBH in the PIM<sub>2</sub> membrane model were also investigated utilizing MD simulations.

### 3.2. BH and NBH effects in the PIM<sub>2</sub> membrane model: MD simulation results

Three systems were studied by MD: the PIM<sub>2</sub> membrane in water (PIM<sub>2</sub> control), membrane with BH (PIM<sub>2</sub>-BH) and membrane with NBH (PIM<sub>2</sub>-NBH). The analyses were conducted utilizing the 100 ns MD production phase for all three systems, considering the final conformations obtained. The RMSD, partial mass density, atomic distances, deuterium order parameters, lateral diffusion and membrane thickness were calculated to evaluate the effects and behavior that the BH and NBH molecules had in the systems.

#### 3.2.1. RMSD

The RMSD of the PIM<sub>2</sub> membrane model in the presence of BH and NBH is shown in Fig. 5.

The RMSD of the lipids contained in the system was calculated every 2 ps along the entirety of the molecular dynamics simulation to assess the deviation of the atomic positions during the process, providing insights of the structural stability of the three systems. It was observed that all three systems began to stabilize at around 40 ns into the simulation. The PIM<sub>2</sub> control had the highest values of RMSD, reaching values of 2 nm before 100 ns. This could indicate higher instability and more

conformational changes in the positions of lipid atoms during MD simulations. Although all systems displayed fluctuations equivalent to or above 1 nm, both PIM<sub>2</sub>-BH and PIM<sub>2</sub>-NBH systems exhibited the most consistent stability throughout the entire 100 ns production. BH started stabilizing with a RMSD around 1 nm, while NBH started at approximately 1.2 nm. This analysis indicates that the interactions in both systems play a significant role in maintaining their structural stability during the simulation, leading to a stabler system compared to the PIM<sub>2</sub> control. Considering this, to obtain information related to the BH and NBH locations in the PIM<sub>2</sub> membrane and compare it to the results obtained with ASO MLVs, the partial density and atomic distance of both molecules from the membrane-specific atoms were investigated, as follows.

#### 3.2.2. Partial density

The partial density of PIM<sub>2</sub> systems in the absence (control) and in the presence of BH and NBH is shown in Fig. 6.

The partial density analysis provides valuable information regarding the spatial arrangement of the molecules within the lipid bilayer. The partial density of the systems in Fig. 6 shows that at 100 ns, the distribution of NBH molecules is closer to the membrane surface (toward lipid headgroups), while the BH molecules stay toward the lipid acyl chains. In no system was there a presence of water in the hydrophobic center of the membrane, located in the acyl chains in the lipid tails. These results agree with our expectations of the behavior of the molecules in the respective systems. The preferential locations of NBH, toward the lipid headgroups, and BH, toward the lipid acyl chains, can significantly influence the overall distribution and stability of the systems. Atomic distance calculations were then performed to obtain more details related to the location of BH and NBH in the membrane. The partial density was also plotted separately by structure and included in the supplementary material, Figs. S11 to S14.

#### 3.2.3. Atomic distance

During the 100 ns simulations, the atomic distances between the N-group in BH and NBH and specific atoms of PIM<sub>2</sub> (C3, C6, C28, C40, O5, O6, O14 and O21, shown in Fig. 7) were calculated to analyze the overall location of the molecules of BH and NBH relative to the lipids present in the membrane. The average atomic distance values between PIM<sub>2</sub>-BH and PIM<sub>2</sub>-NBH are shown in Fig. 8. The algorithm developed to calculate these atomic distances is detailed in the supplementary material of this article (Section 1.1).

The minimum, maximum and average distance values are presented in Table 2. In the PIM<sub>2</sub>-BH system, the distances between BH and the lipid atoms showed smaller values for O6 and O5, which could be related to the proximity of the molecule to the phosphate group in the lipid composition (see Figs. 7 and 8). The average distance between BH and the remaining atoms followed the sequence C6 (located in the carbonyl group related to the acyl chain 2) < O21 (located in the mannosyl group) < C3 (located in the carbonyl group related to the acyl chain 1) < O14 (located in the mannosyl group) < C28 (located in acyl chain 2) < C40 (located in acyl chain 1). On the other hand, among all the PIM<sub>2</sub> atoms, NBH seems to be closer to both mannosyl oxygens (O21 and O14) than to the phosphate atoms (O5 and O6). Thus, the location of BH and NBH seems to be similar to those suggested in the ASO MLV model, considering the expressive interaction of BH with the lipid phosphate group and of NBH with the groups closer to the membrane surface (mannosyl and choline, considering PIM<sub>2</sub> and ASO models, respectively). Here, it is interesting to note that the distances between BH and the two carbonyl groups of PIM<sub>2</sub> (C6 and C3) are very similar to those described for one of the mannosyl oxygens (O21). This was not observed in the NBH results. These data may be correlated to the question proposed in Section 3.1.1, reinforcing that the nitro group may be responsible for a reorientation of NBH which differs from the BH one in both lipid models. Also, the BH seems to cross the lipid carbonyl groups and the oxygens of the mannosyl region, maybe reorienting the PIM<sub>2</sub>

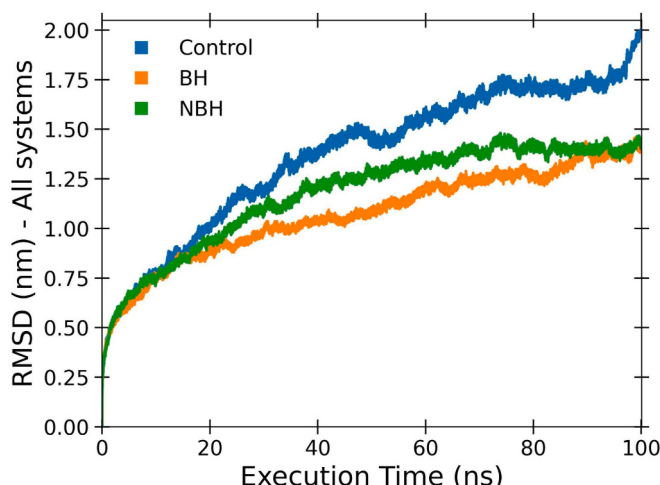


**Fig. 5.** Root Mean Square Deviation (RMSD) of the PIM<sub>2</sub> system in the absence (control, blue curve) and in the presence of BH (orange curve) and NBH (green curve), in a 100 ns MD simulation. The Y-axis represents the RMSD in nm and the X-axis shows the MD time frame in ns.

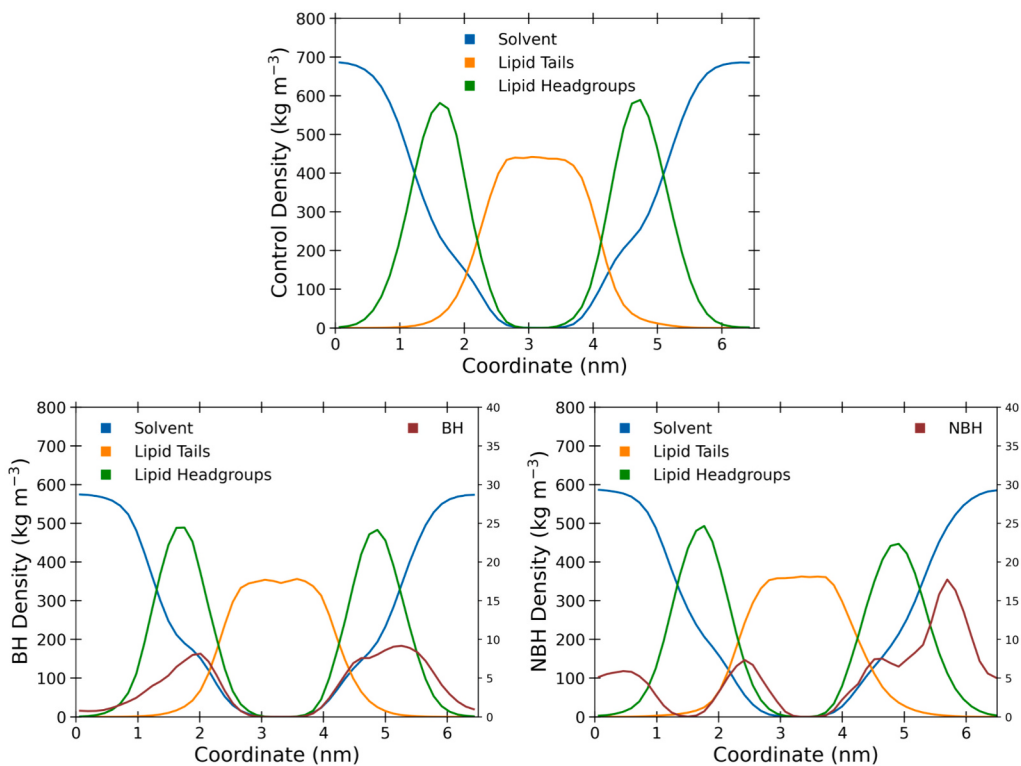


**Fig. 6.** Density profiles of PIM<sub>2</sub> control, PIM<sub>2</sub> BH and PIM<sub>2</sub> NBH, calculated at the end of the production run. For all the graphs, the horizontal axis presents the coordinates in nm and the vertical axis shows the density in kg m<sup>-3</sup>. The two bottom graphics have a right axis with a different scale for representing the density of hydroxamic acid.

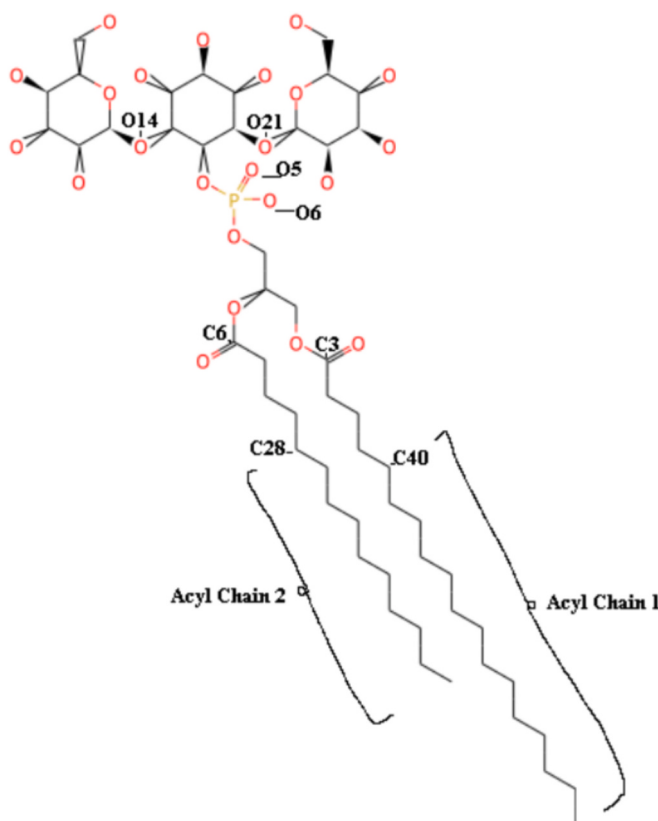


**Fig. 7.** Location of the specific lipid atoms used as a reference for the atomic distance studies: C3, C6, C28, C40, O5, O6, O14 and O21.

molecule, which may not happen in the NBH system. This may reflect different effects in the methylene chains of the lipid. Thus, these effects were investigated by studies of deuterium order parameters, as follows. To further enhance the visibility distance and diffusion analysis of the hydroxamic acids, snapshots of both the PIM<sub>2</sub>-BH and PIM<sub>2</sub>-NBH systems were taken from 0 ns to 100 ns. These snapshots are included in Section 2.5 of the supplementary material as Figs. S15 to S26.

### 3.2.4. Deuterium order parameters

The deuterium order parameters related to the acyl chains of PIM<sub>2</sub> membrane, in the absence (control) and in the presence of BH and NBH are shown in Fig. 9.

Deuterium order parameters were calculated to analyze the effects of BH and NBH in the order of the acyl chains (1 and 2) of the bilayer system. For both PIM<sub>2</sub> acyl chains, BH simulation results showed smaller values of deuterium order parameter than the control (28.18 % lower in Chain 1 and 27.83 % lower in Chain 2). This reinforces a disorder effect in the membranes promoted by BH, which was also observed for the ASO MLV model. The higher mobility of the PIM<sub>2</sub>-BH system may be attributed to the BH reorientation effect in the membrane, as well as to its location, which is lower when compared to the NBH location. The deuterium order parameter curves in NBH showed higher values than the control (9.65 % higher in Chain 1 and 7.66 % higher in Chain 2), suggesting a restriction of acyl chain motions. These results corroborate FTIR and NMR data related to ASO MLVs, as well as reinforce the influence of the higher location in NBH and small effect in membrane reorientation of NBH compared to BH. Thus, in PIM<sub>2</sub>, it seems that the position and orientation of these drugs in the membranes have an important influence on the order of lipid acyl chains. Additional deuterium order parameter plots were created, including error bars and average values of Scd, calculated every 2 ns from 10 to 100 ns of the molecular dynamic simulation. These plots are included in the supplementary material as Figs. S3 to S10 in Section 2.4.

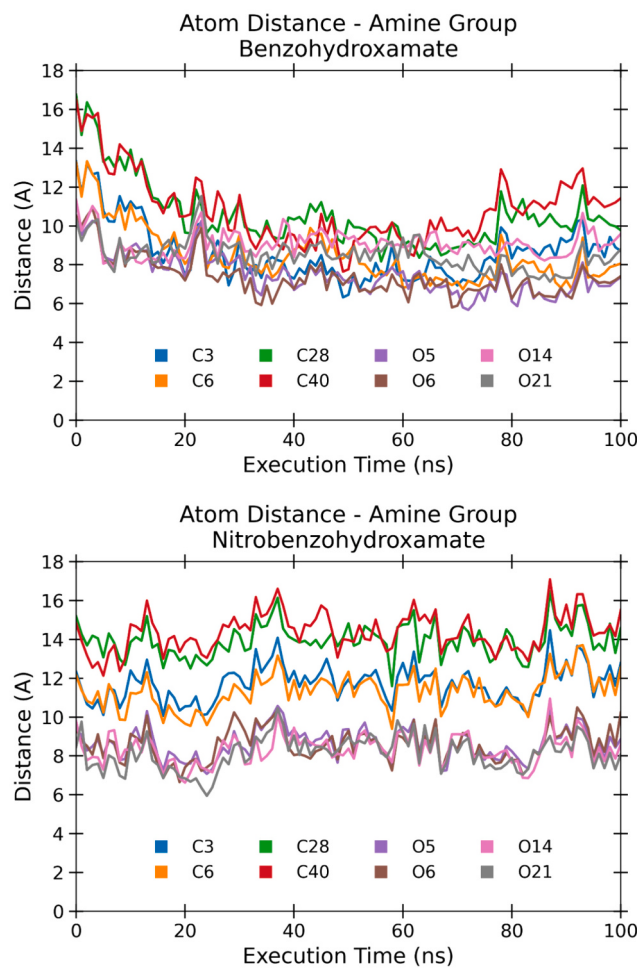


**Fig. 8.** Average nitro-group distance from benzohydroxamate (BH) and nitrobenzohydroxamate (NBH) to specific lipid atoms. Calculated with the average distance of the nitro-group in BH and NBH from all 12 molecules to the atoms of interest.

**Table 2**

Minimum, maximum and average distance values ( $\text{\AA}$ ) between the nitro group and each of the chosen atoms in the PIM<sub>2</sub> system containing BH (PIM<sub>2</sub>-BH) and that containing NBH (PIM<sub>2</sub>-NBH) during the 100 ns production run.

Atom	Minimum distance Ångström ( $\text{\AA}$ )		Maximum distance Ångström ( $\text{\AA}$ )		Average distance Ångström ( $\text{\AA}$ )	
	PIM <sub>2</sub> - BH	PIM <sub>2</sub> - NBH	PIM <sub>2</sub> - BH	PIM <sub>2</sub> - NBH	PIM <sub>2</sub> - BH	PIM <sub>2</sub> - NBH
C3	6.318	10.057	13.315	14.466	8.631	11.731
C6	6.733	9.390	13.332	13.705	8.487	11.336
C28	8.168	11.590	16.747	16.477	10.576	13.964
C40	7.642	12.127	16.492	17.092	10.847	14.376
O5	5.673	7.075	10.519	10.569	7.508	8.635
O6	5.798	6.646	10.903	10.493	7.386	8.575
O14	7.789	6.619	11.337	10.947	9.090	8.333
O21	7.123	5.943	11.534	10.451	8.514	8.128

### 3.2.5. Lateral diffusion

The lateral diffusion of PIM<sub>2</sub> was investigated in order to obtain information about the effect of BH and NBH in the PIM<sub>2</sub> fluidity and correlate it to the effects observed in the degree of the order of ASO MLVs. The lateral diffusion of the specific PIM<sub>2</sub> atoms of C3, C6, C28 and C40 (please see Fig. 7), and that related to the phosphorus (P1), are shown in Fig. 10.

The mean square displacement (MSD) is a measure used in the study

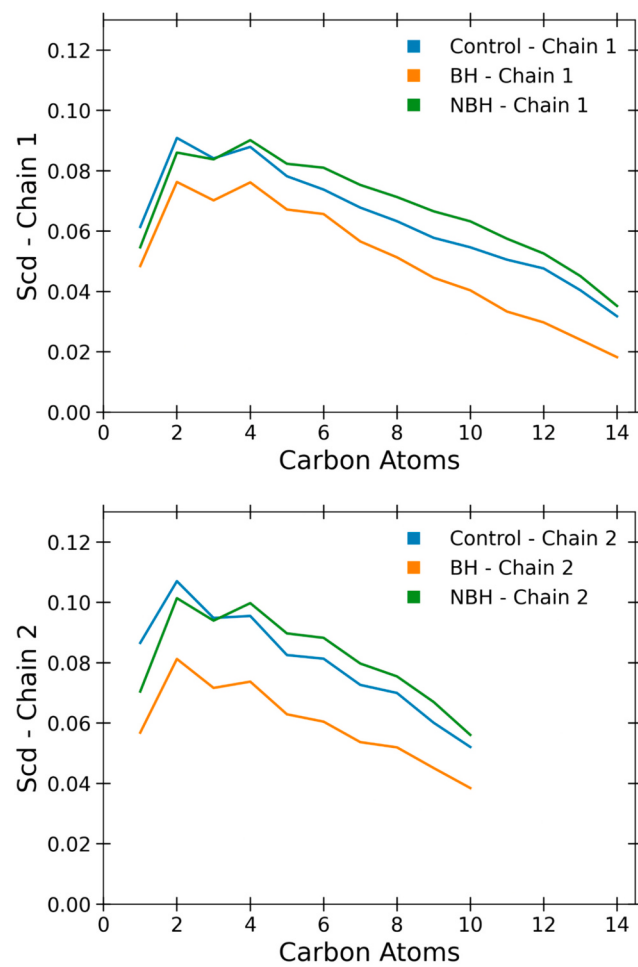


**Fig. 9.** Deuterium order parameters of acyl chains 1 (top) and 2 (bottom) for PIM<sub>2</sub> control, and PIM<sub>2</sub> systems containing BH and NBH.

of particle or atom movement. In the MD simulations, it provides insights into the dynamics and mobility of particles within a system. It was calculated the MSD of PIM<sub>2</sub> C3, C6, C28 and C40 as well as P atoms to analyze the overall lateral diffusion of the systems. The lateral diffusion was higher in the control system (values going from 0 to 14 in the Y-axis) containing only the membrane, water and Na<sup>+</sup> ions, going above  $12 \times 10^{-5} \text{ cm}^2/\text{s}$  at 94 ns. The lateral diffusion of NBH was higher than BH in all the atoms of interest, reaching values higher than  $7.4 \times 10^{-5} \text{ cm}^2/\text{s}$ , while BH had the highest value of  $5.3 \times 10^{-5} \text{ cm}^2/\text{s}$  in the C40 atom. Higher lateral diffusion indicates higher fluidity in the membrane. Thus, when compared with the PIM<sub>2</sub> system (control), both BH and NBH reduced the membrane fluidity.

However, although NBH had increased the motion restriction in the PIM<sub>2</sub> membrane (behavior also observed in ASO MLVs) compared to BH, it promoted the highest lateral diffusion between both drugs. It is known that the lipid lateral diffusion is a consequence of intermolecular interactions in its hydrophobic core which, in turn, is affected by the dipole-induced packing and steric effects [86]. The nitro group of NBH may enhance the dipole-induced packing and the steric effects in the membrane and, as observed in the deuterium order parameter assay, it restricted the motion of the lipid acyl chains. Thus, it was expected that NBH would decrease the lipid lateral diffusion when compared to BH. As the opposite effect was observed for NBH, it is possible that its membrane location in a higher position (compared to BH) may have influenced its lateral diffusion. The location and restriction of BH in the lipid phosphate group, as well as its effect in the membrane reorientation,

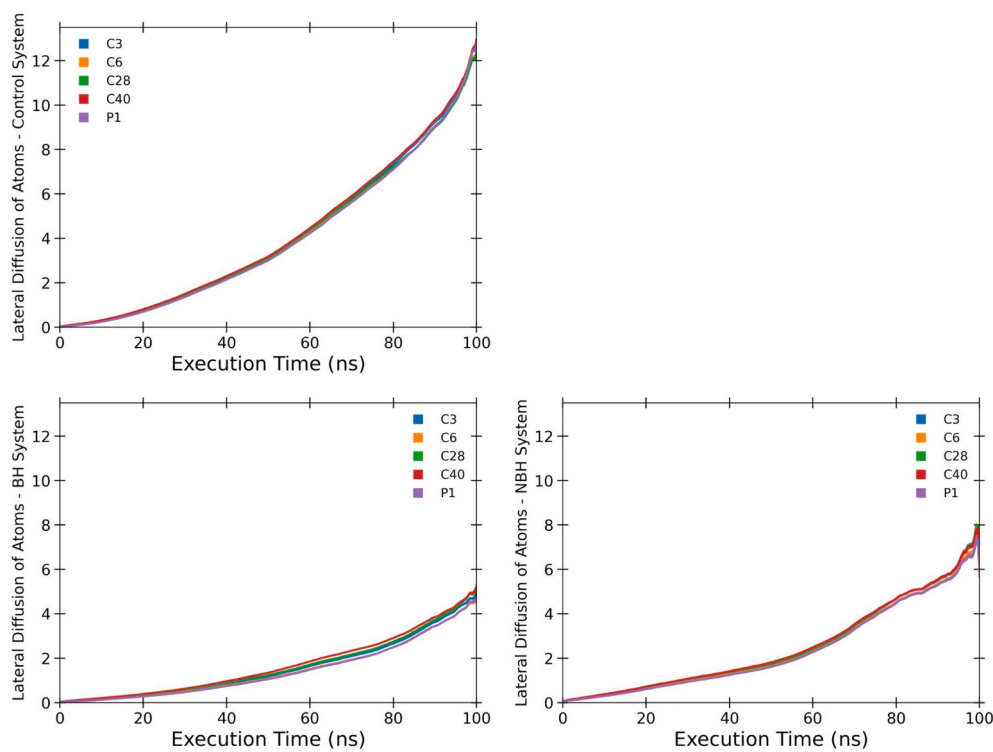


**Fig. 10.** Lateral diffusion of atoms in the PIM<sub>2</sub> system (control) and PIM<sub>2</sub> containing benzohydroxamate (BH) and nitrobenzohydroxamate (NBH).

may have a stronger effect in the lipid lateral diffusion, decreasing it.

#### 3.2.6. Membrane thickness

The thickness of the PIM<sub>2</sub> bilayer systems was measured to provide valuable information about the structural characteristics of the PIM<sub>2</sub> systems, mainly related to packing density. Results are shown in Fig. 11.

The membrane thickness was calculated using the final conformations of the membrane systems at 100 ns using GridMAT-MD and plotted with a python script, with the Z-axis representing the thickness of the membrane. The PIM<sub>2</sub> system (control) had 25 % of its thickness above 3 nm, while the PIM<sub>2</sub>-BH system had 60 % and the PIM<sub>2</sub>-NBH system had 60.25 % of the membrane thickness above 3 nm, respectively. This

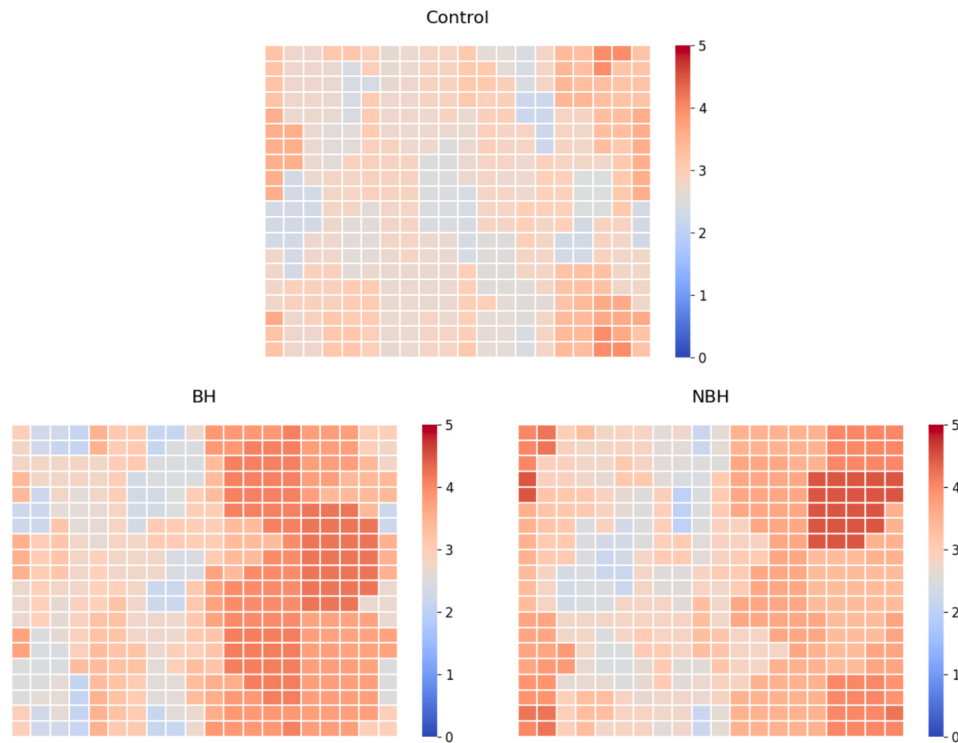


**Fig. 11.** Membrane thickness of PIM<sub>2</sub> control, BH and NBH, calculated utilizing the last conformation obtained (100 ns) for all simulation settings. The Z-axis (coloring) represents the thickness of the systems, while the Y-axis and X-axis are grid points representing positions y and x of the systems in nm.

indicates that both BH and NBH increase the membrane thickness in a similar way (with a difference of only 0.25 %), enhancing it by around 35 % when compared to the control. This increase reflects their ordering effect in the lipid polar region. Notably, the disordering effect of BH in the lipid acyl chains (observed by deuterium order parameter assays) did not have a significant influence on the membrane thickness. This observation could have implications for the behavior and properties of the membranes in each system, as the thickness is an important factor in determining membrane function.

In summary, the RMSD experiments showed a higher stability for the PIM<sub>2</sub> membrane when interacting with both BH and NBH. The partial density and atomic distance studies reinforced that the BH system is located closer to the PIM<sub>2</sub> phosphate group and the NBH seems to be closer to both mannose oxygens. As found for ASO MLVs, NBH seems to be located in a higher position than BH in the PIM<sub>2</sub> membrane. The deuterium order parameter measurements relative to the control (PIM<sub>2</sub> membrane without BH and NBH) showed lower values (by around 20 %) for BH, which reinforces a disturbing effect of BH in both membrane models, since the disordering effect of BH was also observed in ASO MLVs. The highest values of lateral diffusion for NBH were  $2.1 \times 10^{-5}$  cm<sup>2</sup>/s higher than BH. Both BH and NBH increased the membrane thickness by 35 %, showing a global ordering effect of these drugs on it.

#### 4. Conclusions

In this study, the spectroscopic results evidence the preferential location of BH and NBH in ASO MLVs, and the MD simulation data with PIM<sub>2</sub> seem to corroborate them, as also seen in our previous work with mefloquine [3]. Thus, the correlation of the properties of both membrane models is useful to have insights about the mechanisms of action of anti-TB drugs, along with mechanisms related to the synergism of drugs against Mtb. Our results also reflected how the molecular orientation of BH and NBH may reflect in their degree of membrane order, interactions, lateral diffusion, and global fluidity, among other physicochemical properties. Considering that BH and NBH have different locations and affect the behavior of the tested membrane models, it is possible that they may perturb the packing of the bacteria cell envelope, also affecting its function and therapy resistance. It is also possible that BH and NBH affect the performance of their corresponding metal complexes against Mtb. However, more studies are necessary to confirm these hypotheses. Data shown here and in the previous work [3] reinforce that both models, in addition to the molecular interaction and orientation analyses, may be useful in the design and development of new systems to be used in anti-TB therapy, as well as for obtaining insights related to their anti-TB action mechanisms.

#### CRediT authorship contribution statement

**Lucas Thadeu Felipe Kokuszi:** Writing – original draft, Investigation. **Yago Mendes Paes:** Writing – original draft, Investigation. **Aline Loise Santana Faria:** Investigation. **Jesus Alvarado-Huayhuaz:** Writing – original draft, Investigation. **Maurício Dornelles Caldeira Balboni:** Investigation. **Marinalva Cardoso dos Santos:** Writing – original draft, Investigation. **Sandra Cruz dos Santos:** Writing – original draft, Investigation. **Juliano Rosa de Menezes Vicenti:** Investigation, Conceptualization. **Alexandre Luis Parize:** Investigation. **Adriano Velasque Werhli:** Writing – review & editing, Supervision. **Karina dos Santos Machado:** Writing – review & editing, Supervision. **Vânia Rodrigues de Lima:** Writing – review & editing, Supervision, Funding acquisition, Conceptualization.

#### Declaration of competing interest

The authors declare the following financial interests/personal relationships which may be considered as potential competing interests: Lucas Thadeu Felipe Kokuszi reports financial support was provided by

National Council for Scientific and Technological Development. Marinalva Cardoso dos Santos reports financial support was provided by Coordination of Higher Education Personnel Improvement. Yago Mendes Paes reports financial support was provided by Foundation for Research Support of Rio Grande do Sul State. If there are other authors, they declare that they have no known competing financial interests or personal relationships that could have appeared to influence the work reported in this paper.

#### Acknowledgements

The authors are thankful to the National Council for Scientific and Technological Development (CNPq), Coordenação de Aperfeiçoamento de Pessoal de Nível Superior (CAPES) and Fundação de Amparo à Pesquisa do Estado do Rio Grande do Sul (FAPERGS) for providing financial support. The authors also would like to thank the Analytical Integrated Center of the Federal University of Rio Grande (CIA/FURG) for NMR and DSC analyses. This work is dedicated to Juliano Rosa de Menezes Vicenti (PhD), *in memoriam*, to start and help to concretize this research dream.

#### Appendix A. Supplementary data

Supplementary data to this article can be found online at <https://doi.org/10.1016/j.bbamem.2024.184378>.

#### References

- [1] G.A. Libreros-Zúñiga, C. dos Santos Silva, R.S. Ferreira, M.V. Bertacine Dias, Structural basis for the interaction and processing of  $\beta$ -lactam antibiotics by L, D-transpeptidase 3 (LdtMt3) from *Mycobacterium tuberculosis*, ACS Infect. Dis. Ther. 5 (2018) 260–271, <https://doi.org/10.1021/acsinfedis.8b00244>.
- [2] I.L.D. Moutinho, Tuberculose: aspectos imunológicos na infecção e na doença, RMMG 21 (2011) 42–48. <https://pesquisa.bvsalud.org/portal/resource/pt/lil-589462>.
- [3] M.C. dos Santos, J.L.R. Scaini, M.V.C. Lopes, B.G. Rodrigues, N.O. Silva, C.R. L. Lopes, S.C. dos Santos, K. Machado, A.V. Werhli, P.E.A. da Silva, M.C. S. Lourenço, E.T. da Silva, M.V.N. de Souza, V.R. de Lima, R.S.B. Gonçalves, Mefloquine synergism with anti-tuberculosis drugs and correlation to membrane effects: biologic, spectroscopic and molecular dynamics simulations studies, Bioorg. Chem. 110 (2021) 104786–104796, <https://doi.org/10.1016/j.bioorg.2021.104786>.
- [4] S. Wellington, D.T. Hung, The expanding diversity of *Mycobacterium tuberculosis* drug targets, ACS Infect. Dis. 4 (2018) 696–714, <https://doi.org/10.1021/acsinfedis.7b00255>.
- [5] WHO, World Health Organization: Global tuberculosis report 2021. <https://www.who.int/publications-detail-redirect/9789240037021/>, 2021 (accessed 14 September 2023).
- [6] A. Zumla, P. Nahid, S. Cole, Advances in the development of new tuberculosis drugs and treatment regimens, Nat. Rev. Drug Discov. 12 (2013) 388–404, <https://doi.org/10.1038/nrd4001>.
- [7] P.J. Brennan, Structure, function, and biogenesis of the cell wall of *Mycobacterium tuberculosis*, Tuberculosis 83 (2003) 91–97, [https://doi.org/10.1016/S1472-9792\(02\)00089-6](https://doi.org/10.1016/S1472-9792(02)00089-6).
- [8] A.K. Mishra, N.N. Criessen, B.J. Appelmelk, G.S. Besra, Lipooligosaccharides and related glycoconjugates: structure, biogenesis and role in *Mycobacterium tuberculosis* physiology and host-pathogen interaction, FEMS Microbiol. Rev. 35 (2011) 1126–1157, <https://doi.org/10.1111/j.1574-6976.2011.00276.x>.
- [9] S.M. Gygli, S. Borrell, A. Trauner, S. Gagneux, Antimicrobial resistance in *Mycobacterium tuberculosis*: mechanistic and evolutionary perspectives, FEMS Microbiol. Rev. 41 (2017) 354–373, <https://doi.org/10.1093/femsre/fux011>.
- [10] M.J.A. Reid, N. Arinaminpathy, A. Bloom, B.R. Bloom, C. Boehme, R. Chaisson, D. P. Chin, G. Churchyard, H. Cox, L. Ditiu, M. Dubal, J. Farrar, A.S. Fauci, E. Fekadu, P.I. Fujiwara, T.B. Hallett, C.L. Hanson, M. Harrington, N. Herbert, P.C. Hopewell, C. Ikeda, D.T. Jamison, A.J. Khan, I. Koek, N. Krishnan, A. Motsoaledi, M. Pai, M. C. Ravaglione, A. Sharman, P.M. Small, S. Swaminathan, Z. Temesgen, A. Vassall, N. Venkatesan, K. van Weezenbeek, G. Yamey, B.D. Agins, S. Alexandre, J. R. Andrews, N. Beyeler, S. Bivol, G. Brigden, A. Cattamanchi, D. Cazabon, V. Crudo, A. Daftary, P. Dewan, L.K. Doepel, R.W. Eisinger, V. Fan, S. Fewer, J. Furin, J.D. Goldhaber-Fiebert, G.B. Gomez, S.M. Graham, D. Gupta, M. Kameene, S. Khaparde, E.W. Mailu, E.O. Masini, L. McHugh, E. Mitchell, S. Moon, M. Osberg, T. Pande, L. Prince, K. Rade, R. Rao, M. Remme, J.A. Seddon, C. Selwyn, P. Shete, K.S. Sachdeva, G. Stallworthy, J.F. Vesga, V. Vilc, E.P.O. Goosby, Building a tuberculosis-free world: The Lancet Commission on tuberculosis, Lancet 393 (2019) 1331–1384, [https://doi.org/10.1016/S0140-6736\(19\)30024-8](https://doi.org/10.1016/S0140-6736(19)30024-8).
- [11] E. Adıguzel, F. Yilmaz, M. Emirik, M. Ozil, Synthesis and characterization of two new hydroxamic acids derivatives and their metal complexes, an investigation on the keto/enol, E/Z and hydroxamate/hydroximate forms, J. Mol. Struct. 1127 (2017) 403–412, <https://doi.org/10.1016/j.molstruc.2016.07.081>.

- [12] B.L. Gonçalves, D.F. Ramos, P.C.B. Halicki, P.E. Almeida da Silva, J.R. de Menezes Vicenti, Synthesis, modeling and biological activity of new zinc (II) hydroxamates against streptococcus pneumoniae, *CDC* 22 (2019) 100240–100249, <https://doi.org/10.1016/j.cdc.2019.100240>.
- [13] E.M.F. Muri, M.J. Nieto, R.D. Sindelar, J.S. Williamson, Hydroxamic acids as pharmacological agents, *Curr. Med. Chem.* 9 (2002) 1631–1653, <https://doi.org/10.2174/0929867023369402>.
- [14] T.S. Coelho, P.C.B. Halicki, L. Silva Jr., J.R. de Menezes Vicenti, B.L. Gonçalves, P. E. Almeida da Silva, D.F. Ramos, Metal-based antimicrobial strategies against intramacrophage *Mycobacterium tuberculosis*, *Lett. Appl. Microbiol.* 71 (2020) 146–153, <https://doi.org/10.1111/lam.13298>.
- [15] R. Galindo-Murillo, L.E. Aguilar Suárez, J. Barroso-Flores, A mixed DFT-MD methodology for the *in silico* development of drug releasing macrocycles. Calix and thia-calix[N]arenes as carriers for Bosutinib and Sorafenib, *J. Comput. Chem.* 37 (2016) 940–946, <https://doi.org/10.1002/jcc.24281>.
- [16] R. Galindo-Murillo, M.E. Sandoval-Salinas, J. Barroso-Flores, In silico design of monomolecular drug carriers for the tyrosine kinase inhibitor drug imatinib based on calix- and thiocalix[n]arene host molecules: a DFT and molecular dynamics study, *J. Chem. Theory Comput.* 10 (2014) 825–834, <https://doi.org/10.1021/ct4004178>.
- [17] Y. Wang, S. Tu, D. Steffen, M. Xiong, Iron complexation to histone deacetylase inhibitors SAHA and LAQ824 in PEGylated liposomes can considerably improve pharmacokinetics in rats, *J. Pharm. Pharm. Sci.* 17 (2014) 583–602, <https://doi.org/10.18433/j3ts4v>.
- [18] H. Daraee, A. Etemadi, M. Kouhi, S. Alimirzalou, A. Akbarzadeh, Application of liposomes in medicine and drug delivery, *Artif. Cells Nanomed. Biotechnol.* 44 (2016) 381–391, <https://doi.org/10.3109/21691401.2014.953633>.
- [19] K. Grave, M.D. Bennett, M. Hogbom, Structure of *Mycobacterium tuberculosis* phosphatidylinositol phosphate synthase reveals mechanism of substrate binding and metal catalysis, *Commun. Biol.* 2 (2019) 1–11, <https://doi.org/10.1038/s42003-019-0427-1>.
- [20] M. Pinheiro, J.J. Giner-Casares, M. Lucio, J.M. Caio, C. Moitinho, J.L.F.C. Lima, S. Reis, L. Camacho, Interplay of mycolic acids, antimycobacterial compounds and pulmonary surfactant membrane: a biophysical approach to disease, *Biochim. Biophys. Acta Biomembr.* 2013 (1828) 896–905, <https://doi.org/10.1016/j.bbamem.2012.09.015>.
- [21] M.M. Moreno, P. Garidel, M. Suwalsky, J. Howe, K. Brandenburg, The membrane-activity of Ibuprofen, Diclofenac, and Naproxen: a physico-chemical study with lecithin phospholipids, *Biochim. Biophys. Acta Biomembr.* 1788 (2009) 1296–1303, <https://doi.org/10.1016/j.bbamem.2009.01.016>.
- [22] M. Traikia, D.E. Warschawski, M. Recouvreur, J. Cartaud, P.F. Devaux, Formation of unilamellar vesicles by repetitive freeze-thaw cycles: characterization by electron microscopy and <sup>31</sup>P-nuclear magnetic resonance, *Eur. Biophys. J.* 29 (2000) 184–195, <https://doi.org/10.1007/s002490000077>.
- [23] D.W. Borhani, D.E. Shaw, The future of molecular dynamics simulations in drug discovery, *J. Comput. Aided Mol. Des.* 26 (2012) 15–26, <https://doi.org/10.1007/s10822-011-9517-y>.
- [24] F. Szoka, D. Papahadjopoulos, Procedure for preparation of liposomes with large internal aqueous space and high capture by reverse-phase evaporation, *Proc. Natl. Acad. Sci. USA* 75 (1978) 4194–4198, <https://doi.org/10.1073/pnas.75.9.4194>.
- [25] O. Mertins, M. Sebben, A.R. Pohlmann, N.P. da Silveira, Production of soybean phosphatidylcholine-chitosan nanovesicles by reverse phase evaporation: a step by step study, *Chem. Phys. Lipids* 138 (2005) 29–37, <https://doi.org/10.1016/j.chemphyslip.2005.07.004>.
- [26] D.G. Fatouros, S.G. Antimisiaris, Effect of amphiphilic drugs on the stability and zeta-potential of their liposome formulations: a study with prednisolone, diazepam, and griseofulvin, *J. Colloid Interface Sci.* 251 (2002) 271–277, <https://doi.org/10.1006/jcis.2002.8432>.
- [27] C. Chen, C.P. Tripp, An infrared spectroscopic based method to measure membrane permeance in liposomes, *Biochim. Biophys. Acta Biomembr.* 1778 (2008) 2266–2272, <https://doi.org/10.1016/j.bbamem.2008.05.010>.
- [28] J. Seelig, <sup>31</sup>P nuclear magnetic resonance and the head group structure of phospholipids in membranes, *Biochim. Biophys. Acta Biomembr.* 515 (1978) 105–140, [https://doi.org/10.1016/0304-4157\(78\)90001-1](https://doi.org/10.1016/0304-4157(78)90001-1).
- [29] R. Koynova, M. Caffrey, Phases and phase transitions of the phosphatidylcholines, *Biochim. Biophys. Acta Rev. Biomembr.* 1376 (1998) 91–145, [https://doi.org/10.1016/S0304-4157\(98\)00006-9](https://doi.org/10.1016/S0304-4157(98)00006-9).
- [30] D.V. Lynch, P.L. Steponkus, Lyotropic phase behavior of unsaturated phosphatidylcholine species: relevance to the mechanism of plasma membrane destabilization and freezing injury, *Biochim. Biophys. Acta Biomembr.* 984 (1989) 267–272, [https://doi.org/10.1016/0005-2736\(89\)90292-7](https://doi.org/10.1016/0005-2736(89)90292-7).
- [31] A.S. Ulrich, M. Sami, A. Watts, Hydration of DOPC bilayers by differential scanning calorimetry, *Biochim. Biophys. Acta Biomembr.* 1191 (1994) 225–230, [https://doi.org/10.1016/0005-2736\(94\)90253-4](https://doi.org/10.1016/0005-2736(94)90253-4).
- [32] C.R.L. de Azambuja Borges, N.O. Silva, M.R. Rodrigues, M.A. Germani Marinho, F. S. de Oliveira, C. Mendes, A.P. Horn, A.L. Parize, D.C. Flores, R.M. Clementin, V. R. de Lima, Dimiristoylphosphatidylcholine/genistein molecular interactions: a physico-chemical approach to anti-glioma drug delivery systems, *Chem. Phys. Lipids* 225 (2019) 104828–104839, <https://doi.org/10.1016/j.chemphyslip.2019.104828>.
- [33] V.R. de Lima, M.S.B. Caro, M.L. Munford, B. Desbat, E. Dufourc, A.A. Pasa, T. B. Creczynski-Pasa, Influence of melatonin on the order of phosphatidylcholine-based membranes, *J. Pineal Res.* 49 (2010) 169–175, <https://doi.org/10.1111/j.1600-079X.2010.0792.x>.
- [34] R.S. de Sousa, A.O.M. Nogueira, V.G. Marques, R.M. Clementin, V.R. de Lima, Effects of  $\alpha$ -oleostearic acid on asolectin liposomes dynamics: relevance to its antioxidant activity, *Bioorg. Chem.* 51 (2013) 8–15, <https://doi.org/10.1016/j.bioorg.2013.08.004>.
- [35] D.M. dos Santos, M.P. Sanches, C.M. Poffo, A.L. Parize, G.J.S. Darelli, V.R. de Lima, Syringic and cinnamic acids antiradical/antioxidant activities as *R. ferruginea* extract components and membrane physico-chemical influence, *J. Mol. Struct.* 1220 (2020) 128749–128759, <https://doi.org/10.1016/j.molstruc.2020.128749>.
- [36] S. Pronk, S. Pál, R. Schulz, P. Larsson, P. Bjelkmar, R. Apostolov, M.R. Shirts, J. C. Smith, P.M. Kasson, D.V.D. Spoel, B. Hess, E. Lindahl, GROMACS 4.5: a high-throughput and highly parallel open source molecular simulation toolkit, *Bioinformatics* 29 (2013) 845–854, <https://doi.org/10.1093/bioinformatics/btt055>.
- [37] J.L.R. Scaini, A.V. Werhli, V.R. de Lima, P.E.A. da Silva, J.R. Bordin, K.S. Machado, All-atoms dynamics model for mycobacterial plasma membrane, *BioRxiv* (2019) 788299–788324, <https://doi.org/10.1101/788299>.
- [38] M.D. Hanwell, D.E. Curtis, D.C. Lonie, T. Vandermeersch, E. Zurek, G.R. Hutchison, Avogadro: an advanced semantic chemical editor, visualization, and analysis platform, *J. Chemother.* 4 (2012) 1–17, <https://doi.org/10.1186/1758-2946-4-17>.
- [39] S. Jo, T. Kim, V.G. Iyer, W. Im, CHARMM-GUI: a web-based graphical user interface for CHARMM, *J. Comput. Chem.* 29 (2008) 1859–1865, <https://doi.org/10.1002/jcc.jcc.20945>.
- [40] F. Sajadi, C.N. Rowley, Simulations of lipid bilayers using the CHARMM36 force field with the TIP3P-FB and TIP4P-FB water models, *PeerJ* 6 (2018) e5472–e5498, <https://doi.org/10.7717/peerj.5472>.
- [41] J. Lee, X. Cheng, J.M. Swails, M.S. Yeom, P.K. Eastman, J.A. Lemkul, S. Wei, J. Buckner, J.C. Jeong, Y. Qi, S. Jo, V.S. Pande, D.A. Case, C.L. Brooks III, Alexander D. Mackrell Jr., J.B. Klauda, W. Im, CHARMM-GUI input generator for NAMD, GROMACS, AMBER, OpenMM, and CHARMM/OpenMM simulations using the CHARMM36 additive force field, *J. Chem. Theory Comput.* 12 (2016) 405–413, <https://doi.org/10.1021/acs.jctc.5b00935>.
- [42] M.J. Hope, M.B. Bally, L.D. Mayer, A.S. Janoff, P.R. Cullis, Generation of multilamellar and unilamellar phospholipid vesicles, *Chem. Phys. Lipids* 40 (1986) 89–107, [https://doi.org/10.1016/0009-3084\(86\)90065-4](https://doi.org/10.1016/0009-3084(86)90065-4).
- [43] D.A. Garcia, S. Quiroga, M.A. Perillo, Flunitrazepam partitioning into natural membranes increases surface curvature and alters cellular morphology, *Chem. Biol. Interact.* 129 (2000) 263–277, [https://doi.org/10.1016/S0009-2797\(00\)00254-4](https://doi.org/10.1016/S0009-2797(00)00254-4).
- [44] A.V. Turina, M.V. Nolan, J.A. Zygaldo, M.A. Perillo, Natural terpenes: self-assembly and membrane partitioning, *Biophys. Chem.* 122 (2006) 101–113, <https://doi.org/10.1016/j.bpc.2006.02.007>.
- [45] S.C. dos Santos, N. Osti Silva, J.B. Espinelli Junior, M.A. Germani Marinho, Z. Vieira Borges, N.B. Caon Branco, F.L. Faita, B.M. Soares, A.P. Horn, A.L. Parize, V.R. de Lima, Molecular interactions and physico-chemical characterization of quercetin-loaded magnetoliposomes, *Chem. Phys. Lipids* 218 (2019) 22–33, <https://doi.org/10.1016/j.chemphyslip.2018.11.010>.
- [46] M. Huang, E. Su, F. Zheng, C. Tan, Encapsulation of flavonoids in liposomal delivery systems: the case of quercetin, kaempferol and luteolin, *Food Funct.* 8 (2017) 3198–3208, <https://doi.org/10.1039/C7FO00508C>.
- [47] H.A. Scheidt, A. Pampel, L. Nissler, R. Gebhardt, D. Huster, Investigation of the membrane localization and distribution of flavonoids by high-resolution magic angle spinning NMR spectroscopy, *Biochim. Biophys. Acta Biomembr.* 1663 (2004) 97–107, <https://doi.org/10.1016/j.bbamem.2004.02.004>.
- [48] K. Kachel, E. Asuncion-Punzalan, E. London, Anchoring of tryptophan and tyrosine analogs at the hydrocarbon-polar boundary in model membrane vesicles, *Biochemistry* 34 (1995) 15475–15479.
- [49] R. Sinha, A. Joshi, U.J. Joshi, S. Srivastava, G. Govil, Localization and interaction of hydroxyflavones with lipid bilayer model membranes: a study using DSC and multinuclear NMR, *Eur. J. Med. Chem.* 80 (2014) 285–294, <https://doi.org/10.1016/j.ejm.2014.04.054>.
- [50] H. Yang, H. Li, L. Liu, Y. Zhou, X. Long, Molecular simulation studies on the interactions of 2,4,6-trinitrotoluene and its metabolites with lipid membranes, *J. Phys. Chem. B* 123 (2019) 6481–6491, <https://doi.org/10.1021/acs.jpcb.9b03033>.
- [51] K.H. Sippel, F. Quiocho, Ion-dipole interactions and their functions in proteins, *Protein Sci.* 24 (2015) 1040–1046, <https://doi.org/10.1002/pro.2685>.
- [52] M.C. dos Santos, Y.M.S. Micheletto, N.P. da Silveira, L. da Silva Pinto, F. C. Giacomelli, V.R. de Lima, T.E.A. Frizon, A.G. Dal-Bó, Self-assembled carbohydrate-based vesicles for lectin targeting, *Colloids Surf. B: Biointerfaces* 148 (2016) 12–18, <https://doi.org/10.1016/j.colsurfb.2016.08.053>.
- [53] M.L. Verdonk, G.J. Boks, H. Kooijman, J.A. Kanter, J. Kroon, Stereochemistry of charged nitrogen-aromatic interactions and its involvement in ligand-receptor binding, *J. Comput. Aided Mol. Des.* 7 (1993) 173–182, <https://doi.org/10.1007/BF00126443>.
- [54] C. Felder, H.-L. Jiang, W.-L. Zhu, K.-X. Chen, I. Silman, S.A. Botti, J.L. Sussman, Quantum/classical mechanical comparison of cation- $\pi$  interactions between tetramethylammonium and benzene, *J. Phys. Chem. A* 105 (2001) 1326–1333, <https://doi.org/10.1021/jp002933n>.
- [55] V.H.G. Martins, M.R. Rodrigues, L.D. Mascarenhas, C.R.L. de Azambuja, J. Londono, V.R. de Lima, The effect of furazolidone on the physico-chemical properties of dimyristoylphosphatidylcholine bilayers: relevance to anti-leishmanial therapy, *J. Mol. Struct.* 1059 (2014) 225–231, <https://doi.org/10.1016/j.molstruc.2013.12.004>.
- [56] R. Ghosh, Phosphorus-31 and deuterium NMR studies of structure and motion in bilayers of phosphatidylcholine and phosphatidylethanolamine, *Biochemistry* 27 (1998) 7750–7758, <https://doi.org/10.1021/bi00420a025>.
- [57] V.R. de Lima, M.S.B. Caro, M.I.B. Tavares, T.B. Creczynski-Pasa, Melatonin location in egg phosphatidylcholine liposomes: possible relation to its antioxidant

- mechanisms, *J. Pineal Res.* 43 (2007) 276–282, <https://doi.org/10.1111/j.1600-079X.2007.00474.x>.
- [58] D. Tretiakova, I.L. Deigen, N. Onishchenko, J. Kuntsche, E. Kudryashova, E. Vodovozova, Phosphatidylinositol stabilizes fluid-phase liposomes loaded with a Melphalan lipophilic prodrug, *Pharmaceutics* 13 (2021) 473–492, <https://doi.org/10.3390/pharmaceutics13040473>.
- [59] P.I. Haris, D.C. Lee, D. Chapman, A Fourier transform infrared investigation of the structural differences between ribonuclease A and ribonuclease S, *Biochim. Biophys. Acta Protein Struct. Mol. Enzymol.* 874 (1986) 255–265, [https://doi.org/10.1016/0167-4838\(86\)90024-5](https://doi.org/10.1016/0167-4838(86)90024-5).
- [60] N. Toyran, F. Severcan, Competitive effect of vitamin D<sub>2</sub> and Ca<sup>2+</sup> on phospholipid model membranes: an FTIR study, *Chem. Phys. Lipids* 123 (2003) 165–176, [https://doi.org/10.1016/S0009-3084\(02\)00194-9](https://doi.org/10.1016/S0009-3084(02)00194-9).
- [61] O. Mertins, P.H. Schneider, A.R. Pohlmann, N.P. da Silveira, Interaction between phospholipids bilayer and chitosan in liposomes investigated by <sup>31</sup>P NMR spectroscopy, *Colloids Surf. B: Biointerfaces* 75 (2010) 294–299, <https://doi.org/10.1016/j.colsurfb.2009.08.048>.
- [62] A.V. Marques, P.M. Trindade Jr., S. Marques, T. Brum, E. Harte, M.O. Rodrigues, M.G. Montes D’Oca, P.A. da Silva, A.R. Pohlmann, I.D. Alves, V.R. de Lima, Isoniazid interaction with phosphatidylcholine-based membranes, *J. Mol. Struct.* 1051 (2013) 237–243, <https://doi.org/10.1016/j.molstruc.2013.08.029>.
- [63] J.A. Berden, P.R. Cullis, D.I. Hoult, A.C. McLaughlin, G.K. Radda, R.E. Richards, Frequency dependence of <sup>31</sup>P NMR linewidths in sonicated phospholipid vesicles: effects of chemical shift anisotropy, *FEBS Lett.* 46 (1974) 55–58, [https://doi.org/10.1016/0014-5793\(74\)80333-9](https://doi.org/10.1016/0014-5793(74)80333-9).
- [64] P.L. Yeagle, W.C. Hutton, C.H. Huang, R.B. Martin, Headgroup conformation and lipid–cholesterol association in phosphatidylcholine vesicles: a <sup>31</sup>P (<sup>1</sup>H) nuclear Overhauser effect study, *Proc. Natl. Acad. Sci. USA* 72 (1975) 3477–3481, <https://doi.org/10.1073/pnas.72.9.3477>.
- [65] J. Schiller, M. Müller, B. Fuchs, K. Arnold, D. Huster, <sup>31</sup>P NMR spectroscopy of phospholipids: from micelles to membranes, *Curr. Anal. Chem.* 3 (2007) 283–301, <https://doi.org/10.2174/15734110782109635>.
- [66] H. Pfeiffer, H. Weichert, G. Klose, K. Heremans, Hydration behaviour of POPC/C12-Bet mixtures investigated by sorption gravimetry, <sup>31</sup>P NMR spectroscopy and X-ray diffraction, *Chem. Phys. Lipids* 165 (2012) 244–251, <https://doi.org/10.1016/j.chemphyslip.2012.01.004>.
- [67] S. Villasmil-Sánchez, A.M. Rabasco, M.L. González-Rodríguez, Thermal and <sup>31</sup>P-NMR studies to elucidate sumatriptan succinate entrapment behavior in phosphatidylcholine/cholesterol liposomes. Comparative <sup>31</sup>P-NMR analysis on negatively and positively-charged liposomes, *Colloids Surf. B: Biointerfaces* 105 (2013) 14–23.
- [68] J.H. Noggle, R.E. Schirmer, The Nuclear Overhauser Effect, Academic Press, New York, 1971, <https://doi.org/10.1002/ange.19730852018>.
- [69] A.C. McLaughlin, P.R. Cullis, M.A. Hemminga, D.I. Hoult, G.K. Radda, G.A. Ritchie, P.J. Seeley, R.E. Richards, Application of <sup>31</sup>P NMR to model and biological membrane systems, *FEBS Lett.* 57 (1975) 213–218, [https://doi.org/10.1016/0014-5793\(75\)80719-8](https://doi.org/10.1016/0014-5793(75)80719-8).
- [70] A. Timoszyk, Z. Gdaniec, L. Latanowicz, The effect of polysialic acid on molecular dynamics of model membranes studied by <sup>31</sup>P NMR spectroscopy, *Solid State Nucl. Magn. Reson.* 25 (2004) 142–145, <https://doi.org/10.1016/j.ssnmr.2003.03.023>.
- [71] S. Garcia-Manyes, G. Oncins, F. Sanz, Effect of ion-binding and chemical phospholipid structure on the nanomechanics of lipid bilayers studied by force spectroscopy, *Biophys. J.* 89 (2005) 1812–1826, <https://doi.org/10.1529/biophysj.105.064030>.
- [72] C.R.L. de Azambuja Borges, L.G. dos Santos, M.R. Rodrigues, R.F. Meneses Rodrigues, E.F. da Silveira, J.H. Azambuja, A.F.C. Flores, A.P. Horn, C. Lima Dora, A.L. Muccillo-Baisch, E. Braganhol, L.S. Pinto, A.L. Parize, V.R. de Lima, Physico-chemical characterization of asolectin–genistein liposomal system: an approach to analyze its in vitro antioxidant potential and effect in glioma cells viability, *Chem. Phys. Lipids* 193 (2015) 24–35, <https://doi.org/10.1016/j.chemphyslip.2015.10.001>.
- [73] W. Hubner, A. Blume, Interactions at the lipid–water interface, *Chem. Phys. Lipids* 96 (1998) 99–123, [https://doi.org/10.1016/S0009-3084\(98\)00083-8](https://doi.org/10.1016/S0009-3084(98)00083-8).
- [74] Z. Arsov, L. Quaroni, Direct interaction between cholesterol and phosphatidylcholines in hydrated membranes revealed by ATR-FTIR spectroscopy, *Chem. Phys. Lipids* 150 (2007) 35–48, <https://doi.org/10.1016/j.chemphyslip.2007.06.215>.
- [75] J.L. Arondo, F.M. Goni, Infrared studies of protein-induced perturbation of lipids in lipoproteins and membranes, *Chem. Phys. Lipids* 96 (1998) (1998) 53–68, [https://doi.org/10.1016/S0009-3084\(98\)00080-2](https://doi.org/10.1016/S0009-3084(98)00080-2).
- [76] H. Sun, D.V. Greathouse, O.S. Andersen, R.E. Koeppe 2nd, The preference of tryptophan for membrane interfaces: insights from N-methylation of tryptophans in gramicidin channels, *J. Biol. Chem.* 283 (2008) 22233–22243, <https://doi.org/10.1074/jbc.M802074200>.
- [77] H.L. Casal, H.H. Mantsch, H. Hauser, Infrared and <sup>31</sup>P-NMR studies of the interaction of Mg<sup>2+</sup> with phosphatidylserines: effect of hydrocarbon chain unsaturation, *Biochim. Biophys. Acta Biomembr.* 982 (1989) 228–236, [https://doi.org/10.1016/0005-2736\(89\)90059-X](https://doi.org/10.1016/0005-2736(89)90059-X).
- [78] F. Severcan, I. Sahin, N. Kazanci, Melatonin strongly interacts with zwitterionic model membranes—evidence from Fourier transform infrared spectroscopy and differential scanning calorimetry, *Biochim. Biophys. Acta Biomembr.* 1668 (2005) 215–222, <https://doi.org/10.1016/j.bbamem.2004.12.009>.
- [79] M. Heréc, A. Islamov, A. Kuklin, M. Gagó, W.I. Gruszecki, Effect of antibiotic amphotericin B on structural and dynamic properties of lipid membranes formed with egg yolk phosphatidylcholine, *Chem. Phys. Lipids* 147 (2007) 78–86, <https://doi.org/10.1016/j.chemphyslip.2007.03.007>.
- [80] V.R. Kodati, R. El-Jastimi, Michel Lafleur, Contribution of the intermolecular coupling and libratory mobility in the methylene stretching modes in the infrared spectra of acyl chains, *J. Phys. Chem.* 98 (1994) 12191–12197, <https://doi.org/10.1021/j100098a012>.
- [81] M. Moser, D. Marsh, P. Meier, K.H. Wassmer, G. Kothe, Chain configuration and flexibility gradient in phospholipid membranes. Comparison between spin-label electron spin resonance and deuteron nuclear magnetic resonance, and identification of new conformations, *Biophys. J.* 55 (1989) 111–123, [https://doi.org/10.1016/S0006-3495\(89\)82784-5](https://doi.org/10.1016/S0006-3495(89)82784-5).
- [82] A. Ferrarini, P.L. Nordio, Diffusion models for the dynamics of flexible molecules, *J. Chem. Soc. Faraday Trans.* 88 (1992) 1733–1746, <https://doi.org/10.1039/FT9928801733>.
- [83] W.C. Hung, F.Y. Chen, H.W. Huang, Order-disorder transition in bilayers of diphyanoyl phosphatidylcholine, *Biochim. Biophys. Acta Biomembr.* 1467 (2000) 198–206, [https://doi.org/10.1016/S0005-2736\(00\)00221-2](https://doi.org/10.1016/S0005-2736(00)00221-2).
- [84] C.-Y. Cheng, J. Song, J. Pas, L.H.H. Meijer, S. Han, DMSO induces dehydration near lipid membrane surfaces, *Biophys. J.* 109 (2015) 330–339, <https://doi.org/10.1016/j.bpj.2015.06.011>.
- [85] Q. Jiao, R. Wang, Y. Jiang, B. Liu, Study on the interaction between active components from traditional Chinese medicine and plasma proteins, *Chem. Cent. J.* 12 (2018) 1–20, <https://doi.org/10.1186/s13065-018-0417-2>.
- [86] Y. Okamoto, T. Motegi, K. Morita, T. Takagi, H. Amii, T. Kanamori, M. Sonoyama, R. Tero, Lateral diffusion and molecular interaction in a bilayer membrane consisting of partially fluorinated phospholipids, *Langmuir* 32 (2016) 10712–10718, <https://doi.org/10.1021/acs.langmuir.6b02874>.